Distinct expression profile reveals glia involvement in the trigeminal system attributing to post-traumatic headache

Gurueswar Nagarajan[1,2], Yumin Zhang[2,*]

[1]Henry M. Jackson Foundation for the Advancement of Military Medicine, 6720A Rockledge Dr, Bethesda, Maryland 20817, USA

[2]Department of Anatomy, Physiology and Genetics, Uniformed Services University of the Health Sciences, 4301 Jones Bridge Road, Bethesda, Maryland 20814, USA

*Corresponding author: Yumin Zhang, MD, PhD, Dept. of Anatomy, Physiology and Genetics, Uniformed Services University of the Health Sciences, 4301 Jones Bridge Road, Bethesda, MD 20814, USA. Email: yumin.zhang@usuhs.edu

Abstract

Post-traumatic headache (PTH) is a common comorbid symptom affecting at least one-third of patients with mild traumatic brain injury (mTBI). While neuroinflammation is known to contribute to the development of PTH, the cellular mechanisms in the trigeminal system crucial for understanding the pathogenesis of PTH remain unclear. A non-invasive repetitive mTBI (4 times with a 24-hour interval) was induced in male mice and effect of mTBI was tested on either bregma or pre-bregma position on the head. Periorbital allodynia and spontaneous pain behavior were assessed using von Frey test and grimace score, respectively. Quantitative PCR was used to assess extent of mTBI pathology. RNA sequencing was performed to obtain transcriptomic profile of the trigeminal ganglion (TG), trigeminal nucleus caudalis (Sp5C) and periaqueductal gray (PAG) at 7 days post-TBI. Subsequently, quantitative PCR, in situ hybridization and immunohistochemistry were used to examine mRNA and protein expression of glia specific markers and pain associated molecules. The repetitive impacts at the bregma, but not pre-bregma site led to periorbital hypersensitivity, which was correlated with enhanced inflammatory gene expression in multiple brain regions. RNA sequencing revealed mTBI induced distinct transcriptomic profiles in the peripheral TG and central Sp5C and PAG. Using gene set enrichment analysis, positive enrichment of non-neuronal cells in the TG and neuroinflammation in the Sp5C were identified to be essential in the pathogenesis of PTH. In situ assays also revealed that gliosis of satellite glial cells in the TG and astrocytes in the Sp5C were prominent days after injury. Furthermore, immunohistochemical study revealed a close interaction between activated microglia and reactive astrocytes correlating with increased calretinin interneurons in the Sp5C. Transcriptomics analysis indicated that non-neuronal cells in peripheral TG and successive in situ assays revealed that glia in the central Sp5C are crucial in modulating

headache-like symptoms. Thus, selective targeting of glia cells can be a therapeutic strategy for PTH attributed to repetitive mTBI.

Keywords: Trigeminal System, TBI, Brainstem, Glia, Pain, Headache.

Background

Mild traumatic brain injury (mTBI) causes a myriad of pathologies and symptoms. Post-traumatic headache (PTH) is one of the underreported comorbid symptoms of mTBI [1,2] and is observed in more than 30% of clinical diagnoses [3–11]. Repetitive head injuries are associated with an increased incidence of chronic pain, including headaches [6] and clinical data shows that the incidence of PTH varies tremendously involving different mechanisms [12]. Over the last two decades, the heterogeneous nature of PTH symptoms has led to increased understanding of different headache classifications [1,2]. In parallel to these classifications, there are multiple PTH phenotypes and pathology associated with the trigeminal system is thought to underlie one of the phenotypes observed in the clinical population. Several theories regarding the central sensitization that triggers headaches, including migraine, have been proposed [13–15]. However, due to profound trigeminal innervation [16], the exact cellular and molecular mechanisms through which trigeminal regions are primed for central pain sensitization of headache after mTBI remain unclear.

Sensory pseudo-unipolar neurons in the trigeminal ganglion (TG) have innervation throughout the head including the facial region, meninges, scalp, cranial bones and neurovasculature [16–19]. These sensory neurons have a tight relationship with satellite glial cells (SGC) [20,21]. Thus, neurons in the TG are prone to primary insults during head injury via the afferent fibers

74 innervating the head and the injury may affect their first-order projections to the trigeminal
75 nucleus caudalis (Sp5C) as well as other regions of the brainstem. However, these brain regions
76 are subject to injury per se due to rotational movement [22,23] which can impact their
77 projections to the other areas of the brain, including periaqueductal gray (PAG), thalamus,
78 parabrachial nucleus, and anterior cingulate cortex. Thus, head injury-induced pathologies in the
79 TG and Sp5C could cause central sensitization in chronic pain conditions [24–28].
80
81 Preclinical models of neurotrauma have been reported for the past several decades [29–31]. Due
82 to the nature of the injury model and heterogenous symptoms associated with trauma [32–34],
83 the underlying cellular and molecular mechanisms of trigeminal pain following head injury
84 remain poorly understood. Recent evidence shows that invasive procedures have a major effect
85 on sensory neurons of the TG [35,36], leading to the development of trigeminal pain [37] and
86 thus, there is a need for non-invasive procedures to study the trigeminal pain pathway associated
87 with mTBI. Here we used repetitive head injury induced by the closed-head impact model of
88 engineered rotational acceleration (CHIMERA) [38] and showed that development of headache-
89 like symptoms depends on the localization of injury/trauma to the head. Using deep sequencing,
90 in situ hybridization and immunohistochemistry, we aimed to understand the cellular and
91 molecular mechanisms, particularly the inflammatory response, underlying the pathogenesis of
92 PTH attributed to repetitive mTBI.

93 **Methods and Materials**

94 **Induction of repetitive mTBI animal model**

95 Two months old male C57BL/6J mice were obtained from Jackson Laboratory and were
96 habituated for a week before experimental procedures. Once habituated, mice were randomized

97 into different groups. Baseline measurements for von Frey and grimace were obtained prior to
98 repeated mTBI. On the day of the mTBI procedure, mice were assimilated in the procedure room
99 for 30 min. Each mouse was anesthetized under 3% isoflurane in an induction box, and was then
100 placed in supine position under 1.5-2% isoflurane on the CHIMERA (Closed-Head Impact
101 Model of Engineered Rotational Acceleration) stage as described [38]. After a stabilized
102 breathing response and within 2-3 min of anesthesia each mouse received a hit from the piston
103 with an energy level of 0.7J. Since the location of mTBI determines the severity of comatose and
104 brainstem pathologies following the injury [39], mice received TBI impacts in either one of the
105 midline positions (pre-bregma and bregma regions, n=6/group) shown in Fig.1. The distance
106 between the two hit positions differed by ~0.5 cm. Immediately following mTBI, each mouse
107 was placed in the supine position on fresh bedding material and their righting reflexes (comatose
108 or time of recovery from mTBI) were recorded. Mice in the sham group (n=6) were placed on
109 the CHIMERA stage with anesthesia and without mTBI for the same 2-3 minutes duration. After
110 gaining consciousness, mice were returned to their respective home cages. Based on preliminary
111 experiments, we have found that mice with repeated mild injury tend to develop allodynia.
112 Hence, the above procedure was repeated once a day for 4 days. All animal procedures were
113 conducted in accordance with the NIH and AVMA guidelines and approved by the Uniformed
114 Services University of the Health Sciences Institutional Animal Care and Use Committee
115 (IACUC).

116 **Behavioral assessment**

117 On the 6th day following the last TBI impact, mechanical allodynia was measured in the
118 periorbital region using von Frey method. Mechanical threshold measurements were obtained
119 using a simplified Chaplan up-down method [124, 125]. Prior to von Frey test, each mouse was

120 tail restrained in a red tube and habituated for 10 minutes once a day for two days. On the test
121 day, a series of calibrated von Frey filaments (Bioseb, France) ranging from 0.02g to 2g were
122 applied to the midline periorbital region between the eyes. Each filament was perpendicularly
123 placed on the midline region and pressed firmly with sufficient force to bend the filament. A
124 positive response was defined as a rapid withdrawal of the head, or shaking of the head, or
125 retrieving back or face wipe. A minimum of 20-30 seconds elapsed between filament tests.

126 To measure spontaneous pain response following mTBI, a separate cohort of mice was tested for
127 grimace using mouse grimace score [40]. Prior to testing on the 5th day after the last mTBI, mice
128 were habituated in plastic animal enclosures (approximately 10 x 20 x 15 cm) for 15 minutes and
129 on test days each mouse was tested for 10 minutes. Baseline and post-injury grimace scores were
130 obtained from several still pictures and if needed, grimace was confirmed from video recordings.
131 Of the 5 standard mouse grimace features, grimace such as periorbital tightening and altered ear
132 positions were prominent in this mouse cohort and were used in the grimace analyses. In a
133 separate cohort to determine long term effect of mTBI, grimace was measured on day 6, day 16
134 and day 22 post mTBI. All tests were performed between 10 AM and 3 PM. The experimenters
135 were blind to the treatment conditions.

136

137 **Quantitative RT-PCR (qPCR)**

138 To determine regional differences in gene expression following mTBI in pre-bregma and bregma
139 positions (n=5-6/group), fresh frozen samples from several brain regions were collected by
140 cryosectioning at 250µm using dissection mentioned above or using Palkovits punch method.
141 We collected different pain-related brain regions, including Sp5C, PAG (described above),
142 parabrachial nucleus/locus coeruleus (PB/LC), and thalamus. Because the parabrachial nucleus
143 (PB) and locus coeruleus (LC) are in close proximity, both PB and LC were collected together

144 during the Palkovits punch method. Further, to identify temporal variations in the gene
145 expression profile, in a separate cohort (n=6-7/group), fresh TG samples were obtained day1 and
146 day 8 after the last mTBI. Total RNA was extracted using Zymo Research spin column as per
147 manufacturer's instructions. Because TG samples are highly myelinated, excess TRI Reagent was
148 used to yield a good amount of RNA. One to two ug of RNA was then reverse transcribed using
149 Maxima First Strand cDNA Synthesis Kit, and qPCR was performed using primer sets for genes
150 listed in Table 1.

151 **Table 1** List of primes used in quantitative PCR

Genes	**Forward primer**	**Reverse Primer**
Gapdh	AGGTCGGTGTGAACGGATTTG	TGTAGACCATGTAGTTGAGGTCA
Gfap	CCTGAGGCAGAAGCTCCAAG	TCTCCTCCTCCAGCGATTCA
Gja1	ACCCAACAGCAGCAGACTTT	GTCTGGGCACCTCTCTTTCA
Slc1a2	AGTCAATGTGGTGGGCGATT	TCGGTGTTGGGAGTCAATGG
Kcnj10	ACCTCAAGGATCTATGGACGAC	AGCTACCAGATACCACACCAC
Egr1	GAGCACCTGACCACAGAGTC	CGAGTCGTTTGGCTGGGATA
Cd68	TGTCTGATCTTGCTAGGACCG	GAGAGTAACGGCCTTTTTGTGA
Aif1	ATCAACAAGCAATTCCTCGATGA	CAGCATTCGCTTCAAGGACATA
Trem2	CTGGAACCGTCACCATCACTC	CGAAACTCGATGACTCCTCGG

152

153 **Bulk RNAseq and gene set enrichment analysis**

154 Seven days following the repetitive mTBI, flash frozen TG (n=3/group), cryo-dissected Sp5C
155 (n=3/group; bregma from -8.15 mm to -7.64 mm and medio-lateral 1.25 mm) and PAG
156 (n=3/group; bregma from -3.4 mm to -4.96 mm and medio-lateral 0.65 mm) were processed for

157 sequencing. RNA-seq was performed at GENEWIZ (Chelmsford, MA). RNA was extracted
158 using Rneasy Plus Universal mini kit and RNA from TG, Sp5C and PAG samples had a
159 RIN>8.4 (TapeStation) and concentrations were determined by Qubit RNA Assay. The
160 following configuration was used for sequencing: Illumina HiSeq 2x150bp paired end
161 sequencing on an average of 35M reads per sample. Deseq2 analysis was performed to identify
162 differentially expressed genes using apeglm algorithm in lfcShrink function [41].

163 Gene set enrichment analyses (GSEA) and KEGG pathway analyses were performed using
164 'clusterprofiler' and curated mouse gene sets from 'msigdbr' libraries obtained from Molecular
165 Signatures Database (MSigDB) were used to identify enriched gene sets in the mTBI group.
166 Gene ontology of biology processing from C5 collections were used for GSEA. Dotplots for the
167 GSEA were obtained using tidyverse's 'ggplot' or 'pathview' and 'enrichplot' bioconductor
168 packages.

169 Due to recent advances in single cell transcriptomics, there is an increased understanding of the
170 TG cell specific gene expression in headache pathology and TG specific cell atlas [35,36].
171 Custom gene sets were built containing gene sets specific for TG cell populations [36]. These
172 custom-built reference gene sets were then used for enrichment analyses to identify specific TG
173 cell types involved in mTBI. We then also performed a meta-analysis to identify commonly
174 expressed genes between the current mTBI dataset and different headache or injury models
175 (induced by cortical spreading depression, inflammatory soup, spared nerve injury, facial lesion
176 and scratch). Because these transcriptomic datasets are from single nuclear RNAseq, pseudobulk
177 differential expression analysis was performed (as described in Harvard Chan Bioinformatics
178 Core for scRNA-seq pseudobulk DE analysis) and Deseq2 tool was used as described above. For

179 meta-analysis we used p-value combined approach using Fishers methods available in
180 metaRNAseq or MetaVolcanoR packages.

181 **In situ hybridization and immunohistochemistry**

182 Based on gene set enrichment analysis and differential expression data, selective genes were
183 used for *in situ* hybridization using RNAscope Multiplex Fluorescent v2 assays (Advanced Cell
184 Diagnostics, Inc, Newark, CA). The hybridization assay was performed according to the
185 manufacturer's instructions. Fresh frozen protocol was used for TG (12um thick sections) and the
186 fixed-frozen protocol was used for the Sp5C (15 um thick sections) with protease treatment for
187 15 min and 30 min, respectively. Localization of markers of satellite glial cells such as Slc1a2
188 (Cat No. 441341), Gfap (Cat No. 313211) and Kcnj10 (Cat No. 458831) were used to identify
189 the specificity of cell types in the TG. To identify the expression levels of mRNA (Gfap - Cat
190 No. 313211) as well as protein in the Sp5C, immunohistochemistry was performed following in
191 situ hybridization using manufacturer’s instructions. Localization of the GFAP was identified
192 using Anti-GFAP (1:500 dilution; Dako Polyclonal Rabbit Z033429-2), followed by rinsing and
193 incubation with a secondary antibody (Alexa-Fluor 488).

194 To determine inflammatory response by assessing microglial activation in the Sp5C, we used
195 CD68 (1:300 dilution; eBioscience FA-11; rat anti-CD68) and Iba1 (1:500 dilution; Novus
196 NB100-1028; goat anti-Iba1) in a separate assay. For assessing inflammation induced pain
197 signaling (see below), we also performed calretinin immunostaining (1:500 dilution; Swant 6B3;
198 goat anti-calretinin) in the Sp5C and co-immunostained with neurofilament L (1:5000, Encor;
199 RPCA-NF-L-Degen) to define the boundaries of the superficial lamina.

200 Imaging of the tissue sections used for quantitative analysis was performed using Zeiss Axioscan
201 Z1 Slide Scanner. Confocal images were obtained using the Zeiss 980 Confocal microscope. To

202 identify the fine cell process, z-stack images at 1-2 µm intervals were acquired and maximal
203 projection was applied to all images. Calretinin intensity measurement was performed using
204 Profile View in Zen Lite 3.9.

205 **Statistical analysis**

206 All analyses were performed using R 4.2.3 (https://www.R-project.org/). Packages in tidyverse
207 library [42] were used for data processing and analyses. Behavioral and quantitative gene
208 expression data among sham, bregma and pre-bregma mTBI groups were analyzed using mixed
209 effect models or analysis of variance (ANOVA). Further, due to variability in between sections,
210 fluorescence intensity within tissue sections was normalized. Quantitative cell counts or intensity
211 of immunostains between sham and mTBI group were analyzed using stats package lm
212 regression model or welsh test using lme4 package. Effects of mTBI were considered significant
213 at an alpha level of 0.05. All datasets were tested for normality assumptions and when
214 assumptions were violated, non-parametric test (Wilcoxon test) was used. All data were
215 represented as mean ± standard error.

216 Results

217 **Periorbital allodynia and spontaneous pain behavior in mice with repetitive mTBI**

218 Acceleration head injury model by CHIMERA resulted in an increased righting reflex on each of
219 the 4 mTBI days, which reflected an increased unconscious state. On average, irrespective of the
220 hit position, the righting reflex of mTBI mice was ~53 seconds more than the sham group ($F(2,$
221 $93) = 7.7$, $p = 0.00079$; Fig. 1b). On each of the four repetitive mTBI days, no significant
222 difference was observed between bregma and pre-bregma hit groups (Additional File 1).

223 In contrast to the increased righting reflex, 6 days after the last mTBI, only mice that received

224 repeated mTBI hits in the bregma position showed significantly reduced mechanical threshold in
225 the periorbital region, compared to the sham group ($F(2, 23) = 9.41$, $p = 0.001$; Fig. 1c). Mice
226 that received repeated mTBI in the pre-bregma position had an estimated coefficient of -0.08 g (p
227 $= 0.59$), whereas the mTBI group in the bregma position had an estimated coefficient of -0.81 g
228 compared to the sham group ($p < 0.01$). Since pre-bregma position hit did not induce periorbital
229 sensitivity, grimace, gene expression and histology were performed in mTBI mice that exhibited
230 periorbital sensitivity from hit in the bregma position. In a separate cohort, where mice received
231 repetitive hits in the bregma position, grimace was measured at 5 days post-injury. Spontaneous
232 pain measured from grimace was significantly increased in the mTBI group compared to shams
233 ($F(1, 15) = 7.118$, $p = 0.01755$; Fig. 1d). Further, a significant increase in grimace was noticed
234 on week 2 and week 3 following mTBI (Additional File 2).

235 **Gene expression in the trigeminal pain regions following mTBI**

236 Next, we used quantitative PCR to determine mRNA expression in several pain associated
237 regions following mTBI in the pre-bregma or bregma positions. Recent evidence shows that
238 Egr1, early growth response 1 - an immediate early gene, is associated with injury to ganglionic
239 cells [35, 43]. To identify whether mTBI induced injury in the TG the expression of Egr1 was
240 examined. Similar to mTBI mice (bregma hit) exhibiting mechanical allodynia, only the mTBI
241 bregma group showed increased Egr1 mRNA expression in the TG ($p = 0.018$, Fig. 2a)
242 compared to the sham group. Since gliosis and neuroinflammation are the primary sequelae to
243 injury, we also examined generic astrocytes (Gfap) and activated microglia/macrophage (Aif1,
244 Cd68, Trem2) markers in different brain regions including the Sp5C, PAG, PB/LC and thalamus.
245 As anticipated, different regions had differential expression of these genes (Fig. 2b) and the
246 expression levels of these markers were considerably higher in the bregma hit group ($p = 1.48e$-

247 07) than the pre-bregma hit group ($p = 0.00579$), which were both greater than the expression in
248 the sham group. In particular, the markers for microglia/macrophages were upregulated in the
249 Sp5C compared to PAG, PB/LC and thalamus, while the astrocyte marker gene expression was
250 highly upregulated in the PAG compared to Sp5C, PB/LC and thalamus.

251 **Regional transcriptomics and gene set enrichment analysis following mTBI**

252 Following the initial gene expression analyses, three pain related regions (TG, Sp5C and PAG)
253 from bregma hit position were sequenced for subsequent analyses. As expected, transcriptomics
254 data obtained from the TG, Sp5C and PAG revealed distinct gene expression profiles (Fig. 3a).
255 More than 70% of the variance was observed between peripheral (TG) and central (Sp5C/PAG)
256 regions. Whereas, within the brain, 21% variance was observed between the Sp5C and PAG.
257 Similarly, the number of differentially expressed genes varied between regions (with log fold
258 change $> \pm 1$, p-adjusted < 0.05 and base mean count >10). Specifically, differential expression
259 of 4862 genes between TG and Sp5C, 5268 genes between TG and PAG and, within the brain,
260 2056 genes between Sp5C and PAG were noted.

261 Gene set enrichment analyses showed a distinct profile between TG and Sp5C or PAG following
262 mTBI. Although gene sets involved in cell differentiation, tissue repair and remodeling were
263 commonly expressed following mTBI, gene sets related to immune functions were suppressed in
264 the TG but not in the Sp5C or PAG (Fig. 3b-d, Additional File 3). Particularly, following mTBI,
265 gene sets from biological processes of gene ontology showed decreased enrichment (negative
266 sign of normalized enrichment score) of the following GO terms: B cells, T cells, leukocytes,
267 cellular defense response, response to virus, defense response to bacteria, and response to
268 interferon gamma in the TG. Nonetheless, postsynaptic regulation, regulation of ion transport,
269 neuropeptide signaling pathway, and neural precursor of cell proliferation were enriched in the

270 TG of mTBI mice.

271 In contrast to the TG, with an exception of a few, the majority of the gene sets in the Sp5C of
272 medulla and the PAG of the midbrain, were enriched 7 days following mTBI. The only gene
273 sets with negative enrichment score in the Sp5C following TBI were related to microtubule
274 organization which includes axoneme assembly, cilium movement, flagellum dependent cell
275 motility, and microtubule bundle formation. In the PAG, only the gene set related to
276 ensheathment of neurons was negatively enriched. Full list of enriched gene sets obtained from
277 GSEA analyses from all the regions were presented in Additional File 3.

278 **mTBI induced TG specific gene set enrichment analysis and meta-analysis**

279 A GSEA analysis using custom gene sets specific for TG cell types [35,36] showed that non-
280 neuronal cells were highly enriched compared to neuronal cells following mTBI (Fig. 4a).
281 Particularly, a positive enrichment score was identified for fibroblast, myelinated schwann cells
282 ($p < 0.05$) and satellite glial cells ($p = 0.18$). While immune cells and neurons (somatostatin,
283 neurofilament cluster - NF 1-3, non-peptidergic, cLTMRs) specific gene sets showed negative
284 enrichment ($p < 0.05$). Enrichment of fibroblast and satellite cells was consistent with other
285 headache models, such as migraine induced by cortical spreading depression (CSD) or
286 inflammatory soup (IS) [36].

287 Secondly, the overlapping genes between mTBI and other headache or TG injury models were
288 identified using meta-analysis. Because TG samples were collected 7 days following mTBI, only
289 minimal fold changes were noted in the current transcriptomic dataset. Thus, to identify
290 overlapping genes between mTBI and different TG pathology models, a less constraint fold
291 change was used in the current dataset. Since the sequencing datasets from spared nerve injury
292 (SNI), facial lesion and scratch injury [35] were based on TG neuronal population, the number of

293 overlapping genes were reasonably lower compared to those obtained from all cell population in
294 the CSD and IS models [36]. Nonetheless, a majority of the overlapping genes were upregulated
295 (Table 2). A few genes such as Lmo7 (LIM domain 7), involved in protein-protein interaction,
296 overlapped among all models including mTBI, and Nts (neurotensin) overlapped among mTBI,
297 CSD, spared nerve injury, facial injury and scratch. Kccn3 (Potassium Calcium-Activated
298 Channel Subfamily N Member 3) overlapped between mTBI, CSD and IS and belongs to
299 TRPM8 (Transient receptor potential melastatin subtype 8) neuronal cluster. Neuronal injury
300 marker, Atf3 - ATF/CREB family of transcription factors, was overlapped between mTBI, SNI,
301 facial lesion and scratch injury, reflecting Egr1 expression in mTBI. Non-neuronal cell markers
302 particularly for schwann cells, satellite glia, fibroblast and vascular endothelial cells were
303 commonly expressed between mTBI, CSD and IS. Interestingly, satellite glial markers such as
304 Gfap, Iqgap2 (cytoskeleton interacting protein), Slc6a6 (sodium and chloride-ion dependent
305 transporter) were shared among mTBI, CSD and IS. Only a few shared genes (Hmx1, Itga11 and
306 Fhit) were down regulated among mTBI, CSD and IS and were related to distinct neuronal
307 clusters (Table 2).

308 **Table 2.** Comparison of overlapping genes between mTBI and other TG pathology models.

	Up Regulated	**Down Regulated**
Cortical Spreading Depression and mTBI	Gfap, Slc14a1, Cacng4, Iqgap2, Lfng, Unc5d, Lamb3, Adgra1, Caly, Slc6a6, Lmo7, Ptpro, Ecel1, Fam107a, Kcnn3, Nts, Cyp26b1, Lrig1	Fhit, Hmx1, H2-Eb1, Itga11
Inflammatory Soup and mTBI	Fam107a, Plppr4, Gad2, Lamb3, Ccdc153, Cacng4, Il11, Grap, Rasgrp3, Tigd4, Grm1, Etnppl, Ecel1, Tmem30c, Epha10, Cpne7, Pak6, Scd3, Snx30, Htr2c, Shisa3, Rorb, Rgs9, Vwa5b1, Magel2, Slco1c1, Atp10a, Gm6145, Iqgap2, Lhx2, Grm5, Slc30a3, Gli2, Gm14204, Rasal1, Zan, Glra3, Usp54, Cfap65, Gm973,	Hmx1, Fhit, Itga11

	Cyp26b1, Slc6a6, Lrtm2, Gfap, Aldh1a1, Kcnn3, Plk5, Dpep1, Casq1, Lfng, Vsir, Prr5l, Ctxn2, Fzd4, Pou3f3, Lmo7, Gstm1, Lrig1, Dbndd2	
Spared Nerve Injury and mTBI	Atf3, Sema6a, Nts, Lmo7, Ulk4, Map3k19	-
Facial Lesion and mTBI	Atf3, Lmo7, Sez6l, Nts	-
Scratch and mTBI	Atf3, Nts, Sez6l, Lmo7, Myh3, Ptpro	-

Meta-analyses to obtain significantly overlapping genes between different headache models and mTBI were based on Fisher's method.

Although spinal dorsal horn and Sp5C share some similarities in the rexed laminae appearance, due to unique somatotopy and circuitry, Sp5C have quite distinct neurophysiological properties [44]. Since, Sp5C specific transcriptome is not available yet, we utilized the brainstem astrocyte specific gene sets [45] and found that astrocyte specific gene ontology gene sets were enriched in the mTBI (Additional File 4).

Validation of gene expression in the TG

Transcriptomics data identified that gene sets associated with ion channel transport and satellite glial cells were positively enriched in the mTBI mice. Moreover, satellite glia cells have gained attention in the past several years due to their involvement in the pain mechanisms [20,21]. Therefore, we focused on the specific glia markers, Gfap (glial fibrillary acidic protein), Kcnj10 (potassium inwardly rectifying channel subfamily J member 10), Gja1 (gap junction protein, connexin 43), and Slc1a2 (solute carrier family 1 - glial high affinity glutamate transporter). In a separate cohort (n = 7-8/group), quantitative gene expression of satellite glia markers revealed that Gfap and Slc1a2 (Fig. 5a) were upregulated one day after the last mTBI and continued to

326 show increased expression 1-week post mTBI ($p<0.01$). Gja1 was slightly increased on day 1 (p
327 $= 0.0525$), but was significantly upregulated at 1-week post-injury ($p = 0.0339$, Fig. 5a). Using
328 multiplex *in situ* hybridization, mTBI mice showed increased expression of these markers in
329 satellite glia surrounding neurons of the TG (Fig. 5b).

330 **Neuroinflammation in the trigeminal nucleus caudalis**

331 Trigeminal nucleus caudalis showed a wide range of gene expression changes in the
332 transcriptomic data. Importantly, GO terms such as inflammatory response, immune response,
333 cytokine production and regulation of immune system processes were highly enriched in the
334 Sp5C. Diffuse nature of mTBI injury and innervation of primary trigeminal afferents, to the
335 Sp5C, between trigeminal subnuclei and other brainstem regions [46–48], have prompted our
336 investigation of activated microglia using immunohistochemistry in different regions of rostral-
337 caudal extent of the trigeminal Sp5C (Fig. 6). Based on the area and cell number, a significant
338 proliferation of CD68+Iba1+ cells in the white matter, particularly in the spinocerebellar tract
339 (sc, $p = 3.01e-11$; Fig. 6a-c) was noted, while a moderate increase in the tectospinal tract (ts, $p =$
340 0.0038) and pyramidal tract (py, $p = 0.0013$) was observed. In the gray matter, the gracile
341 nucleus (Gr) was found to have significantly increased expression of CD68+Iba1+ cells (Gr, $p <$
342 0.001). Inter reticular nucleus showed a moderate increase in microglia (IRt, $p = 0.0407$) and no
343 differences were noted in the reticular nucleus (MdV, $p=0.623$). Although no significant
344 difference was found in the rostral Sp5C ($p = 0.192$) and caudal Sp5C ($p=0.4$), CD68 intensity
345 within the Iba1+ cells in Sp5C was significantly higher in the mTBI group (Fig. 6d, $P < 0.0001$).
346 Interestingly, these Iba1+ cells were in close association with GFAP+ cells/fibers (Fig. 7f and
347 also see below). Furthermore, morphological differences in microglia were noted in the white
348 matter tracts, gracile nucleus and Sp5C (Additional File 5).

349 Because astrocytes specific gene sets were also enriched in the Sp5C transcriptomic data
350 (Additional File 4) and known to be involved in inflammation [49,50], in parallel to the TG, we
351 also investigated glia expression in the Sp5C of mTBI mice. Similar to gene expression changes
352 in the TG, Gfap mRNA level in the Sp5C was upregulated 1-week post-injury (Fig. 2b and Fig.
353 7c-e). In contrast to the TG, Gfap mRNA expression was found colocalized on long astrocytic
354 processes identified by immunohistochemistry (Fig. 7a-c). Particularly, a fold increase in Gfap
355 mRNA expression was observed at the long processes of GFAP+ astrocytes in mTBI mice (Fig.
356 7e). Although Gfap mRNA was present in the superficial layer of Sp5C and increased in mTBI
357 (Fig. 7c and 7d), due to high density of astrocyte soma in the superficial layer we were unable to
358 quantify Gfap mRNA in GFAP+ soma. Immunostaining also showed that astrocytes in the Sp5C
359 have a distinct expression pattern as they transverse through deep layers of the Sp5C. Compared
360 to the reticular formation (Fig. 7b), only sparse presence of protoplasmic astrocytes were noted
361 in the Sp5C (Fig. 7a-b and Additional File 6). Moreover, in some sections, Gfap+ astrocytes
362 processes were bundled in the sham group while these astrocytes processes were separated in the
363 mTBI group. Although GFAP+ processes traversed from lamina 1 and deeper into lamina 3 (Fig.
364 7d insert), no significant differences were found in the length of GFAP+ processes in the Sp5C
365 between sham and mTBI groups.

366 Due to the increased interest in the astrocyte-microglia interaction in neuroinflammation [51], we
367 also performed triple immunohistochemistry targeting GFAP, Iba1 and CD68+ cells in the
368 brainstem sections. Irrespective of the morphology of GFAP (i.e. either fibrous or protoplasmic
369 astrocytes), a substantial proportion of the GFAP+ fibers or cells were in close contact with
370 Iba1/CD68+ cells (Fig. 7f). Interestingly, lamina 1 of the Sp5C had more GFAP+ fibers in
371 contact with Iba1/CD68+ cells (Fig. 7f - inset 1) than lamina 2 or 3 (Fig. 7f - inset 2-3). Other

372 regions in the brainstem, such as reticular formation and white matter tracts also expressed
373 GFAP+ cells and fibers, respectively, in close proximity to the Iba1/CD68+ cells (Fig. 7f - inset
374 4-6).

375 **Cellular mechanisms of the pain modulation in the trigeminal Sp5C**

376 Since we found increased reactive astrogliosis in the Sp5C of mTBI mice and glutamatergic
377 signaling is well known to be involved in the pain modulation, we next investigated the changes
378 of the glutamate transporter (Slc1a2 gene product of GLT1/EAAT2) in the trigeminal region,
379 Sp5C. Interestingly, the Slc1a2 expression was well defined in the gray matter, particularly in the
380 Sp5C. In contrast to our expectation, the expression of Slc1a2 was ubiquitous without clear
381 boundaries and no identifiable difference was observed between sham and mTBI mice (Fig. 7g).
382 In order to test whether GFAP+ fibers in the Sp5C were in close proximity to Slc1a2 expression,
383 we performed in situ hybridization of Gfap and Slc1a2 combined with GFAP
384 immunohistochemistry, and found that the majority of GFAP+ fibers containing Gfap mRNA
385 were in close proximity to Slc1a2 mRNA expression in lamina 2 and 3 of Sp5C in mTBI mice
386 (Fig. 7h).

387 Further to identify the causal relationship between cellular/molecular changes observed above
388 and headache-like symptoms, we sought to characterize calretinin, a marker involved in
389 allodynia associated with inflammatory pain [52]. We found a reorganization of calretinin
390 immunoreactivity in the Sp5C (Fig. 8a, 8b) where the peak intensity of the calretinin
391 immunoreactivity shifted from outer lamina II to lamina I in the Sp5C of mTBI mice ($p =$
392 0.0136). Moreover, we also identified that the number of calretinin cells differed between rostral-
393 caudal extent of Sp5C and was higher in the mTBI mice (Fig. 8c). Although, the number of
394 calretinin cells were lower in the rostral compared to caudal Sp5C, a significant increase was

395 noted in the rostral Sp5C (p= 0.004) and a non-significant increase was noted in the caudal Sp5C
396 (p = 0.1935).

397 Discussion

398 We found that non-invasive mTBI using the acceleration method induced comatose state as well
399 as headache-like symptoms, which resemble the hallmark comorbid conditions of TBI observed
400 in clinical populations [8,53–56]. Distinct expression profiles and increased inflammation in the
401 pain associated regions following mTBI showed that there was a concerted effort of different
402 brain regions involved in multimodal components of pain [57,58], thereby experiencing both
403 mechanical allodynia as well as spontaneous nociceptive pain response.

404 Repetitive mTBI induced allodynia and grimace

405 In the clinical population, mild head injury has higher prevalence for developing PTH [6,11,59].
406 Similar to clinical cases of mTBI in both nonhuman primates and humans [8,54,56], where
407 patients typically lose consciousness for less than 30 minutes, our mouse model exhibited
408 unconsciousness for a few minutes post-injury. It has been reported that the number of injuries
409 correlates with an increase in persistent headache symptoms [6] and brain pathology [60]. This
410 set the precedent for repetitive head injury in our model where mice developed periorbital
411 sensitivity and grimace over time. In line with this observation in mice, decreased mechanical
412 threshold is one of the characteristics of patients experiencing post-traumatic headache [61,62].
413 Particularly, here we have shown that there are differences in the site of injury on head where
414 mTBI mice exhibit distinct mechanical pain thresholds and varying degrees of inflammatory
415 gene expression in the brain. Although mice were in comatose state after receiving mTBI either
416 in the bregma or pre-bregma position on the dorsum of the head, only mice that received mTBI

417 in the bregma position displayed periorbital sensitivity and grimace thereby mimicking
418 symptoms similar to post-traumatic headache. This could potentially be related to injury to the
419 trigeminal nerve terminals surrounding the head [18,63–65] and these results might explain the
420 heterogeneity involved in mTBI induced symptoms. Effects of mTBI on grimace several days
421 after injury pointed to the fact that mTBI induced by the acceleration method had clinical
422 manifestation where headache symptoms were observed after injury [66]. The profound
423 innervation of the head by the TG, as well as its first and second order connections to the Sp5C,
424 PB, and PAG, suggests a potential role for these regions in the chronification of PTH [57,67,68].

425 **Repetitive mTBI induced differences in gene expression**

426 Having the proof of concept that periorbital sensitivity and grimace become prominent after
427 repetitive mTBI, we investigated gene expression changes in the TG and several other pain
428 related regions. Specifically, sensory information from the trigeminal system is relayed to the
429 ascending pain regions, including PB/LC [65,69,70], PAG [71–73], and the thalamus [74].
430 Similar to existing literature on the difference in the location of impact and regional differences
431 in brain pathology [75,76], we found that non-invasive traumatic injury to the head, only at the
432 bregma region, exhibited prominent changes in Egr1 gene expression in the TG and elevated
433 gene expression of astrocytic and inflammatory markers in the Sp5C, PB/LC, PAG and the
434 thalamus. This enhanced pathology of mTBI in the bregma region was likely due to the
435 proximity of injury to both coronal and sagittal sutures of the cranial vault, neurovasculature, and
436 the biomechanics involved in the trauma [65,77,78]. Together, in our mTBI mouse model, injury
437 to the bregma position of the head has increased TG/brain pathology that likely led to increased
438 headache-like symptoms characterized by periorbital sensitivity and grimace.

439 To comprehensively assess gene expression following mTBI, we performed deep sequencing of

440 the TG, Sp5C, and PAG in mTBI (bregma position) and sham groups. Due to the mild injury
441 model used in this study and sequencing performed in samples collected 7 days post mTBI,
442 fewer than 10 genes resulted in log2 fold change of greater than 1 in the tissues examined.
443 Nonetheless, gene sets enrichment analyses provided an opportunity to understand co-regulated
444 genes from these samples. At 7 days following repetitive mTBI, we found the peripheral TG had
445 a distinct gene expression profile compared to the central Sp5C and PAG. The
446 immunosuppressive state of the TG following mTBI might render it vulnerable to subsequent
447 infection or injury and possibly leading to hyperexcitability of sensory neurons under certain
448 pathogenic conditions [79–82] or even by migraine-like triggers provided several days post
449 injury [83–86]. In contrast to TG, the majority of gene expression in the Sp5C and PAG were
450 upregulated following mTBI. The only difference between the Sp5C and PAG was gene sets
451 involved in the microtubule formation and cilium movement, where these genes were
452 downregulated in the Sp5C and upregulated in the PAG. This difference could be due to the
453 proximity of brainstem Sp5C compared to the PAG, where severe axonal stretching may have
454 led to microtubule disassembly [87,88].

455 To further understand the cellular mechanisms of mTBI induced injury in the TG, we took
456 advantage of recently published TG cell atlas [36]. Using the gene enrichment analyses, it was
457 identified that non-neuronal gene clusters were highly enriched compared to neuronal gene
458 clusters. Enrichment of fibroblast and satellite glial cells was consistent with other mouse
459 headache models (inflammatory soup or cortical spreading depression), but the enrichment of
460 vascular cells shown in the inflammatory soup model [36] was not observed in our mTBI model.
461 We also found that gene sets related to myelinated schwann cells were highly enriched in the
462 mTBI and this could be of importance as schwann cell proliferation has been shown in other

463 nerve injury models [89,90] and might be involved in trigeminal pathology. Further, meta-
464 analysis also revealed a distinct set of genes from this study significantly overlapped with severe
465 injury models such as infra-orbital transection (spared nerve injury), facial lesion or scratch,
466 inflammatory soup or cortical spreading depression models of headache. Injury markers [36]
467 such as Atf3, and Sema6a overlapped between mTBI and severe injury models (spared nerve
468 injury, facial lesion and scratch) reflecting that mTBI induced injury to the TG. Interestingly,
469 Nts, neurotensin, was overlapped in the majority of the injury or headache model, and it has been
470 well documented that neurotensin modulate neuropathic pain [126]. A number of genes related to
471 schwann cells, fibroblast, satellite glia and vascular endothelial cells significantly overlapped
472 between mTBI and headache models (CSD and IS), indicating that non-neuronal cells of the TG
473 have a major role in headache pathology. A few ion channel markers, such as Kccn3 (potassium
474 Calcium-Activated Channel Subfamily N Member 3) and Slc6a6 (sodium and chloride-ion
475 dependent transporter) overlapped between mTBI, CSD and IS, where Kcnn3 has been
476 associated with migraine pathology [127]. Nonetheless, less than 50 genes overlapped between
477 mTBI and other models. As such, mTBI induced a distinct gene expression profile compared to
478 other TG pathology models. Collectively, increased susceptibility of TG and distinct gene
479 expression profile in the TG following mTBI could explain the headache heterogeneity following
480 mTBI in clinical populations [2] and the challenge in translatability using animal models [32].
481 Nevertheless, non-neuronal gene clusters, particularly, satellite glia have gained particular
482 interest for their potential role in headache pathology [20,36].

483 **Glial activation in the trigeminal regions following mTBI**

484 In light of recent evidence, satellite glial cells show a remarkable functional heterogeneity in
485 sensory ganglion [20,91, 21,92]. Here we focused on the expression of specific satellite glial cell

486 markers following mTBI. Consistent with the literature, increased gene expression of Gfap, Gja1
487 and Connexin 43 (Cx43) suggested that mTBI induced increase in satellite glial activity could
488 function as a protective mechanism [93], or to facilitate pain [20,91] as the expression of these
489 genes continued to increase through the post-injury days. In contrast to the existing evidence in
490 other model systems [94–96], we found mTBI increased Kcnj10 expression in the satellite glia
491 surrounding sensory neurons. This might suggest a protective role of glia in the TG through
492 buffering extracellular potassium [97–100] where satellite glial cells could prevent further
493 depolarization of sensory neurons. Additionally, the increased expression of glutamate
494 transporter, Slc1a2, in the mTBI group signifies that glutamate signaling is involved in mTBI
495 induced neuropathic pain as shown in other injury models [101,102]. Since, there is high
496 diversity in satellite glial cells [20,91], increased expression of specific markers found in this
497 study suggests that satellite glial cells of the TG may play a diverse role in mTBI whose precise
498 function in pain is yet to be determined.

499 Compared to the satellite glia cells in the TG, glia in the Sp5C possess a distinct morphology and
500 may have distinct functional roles [103–105]. Due to regional differences in the gene expression
501 pattern [45] and unavailability of trigeminal Sp5C specific transcriptional cell atlas, we applied
502 gene sets (e.g. astrocytes) specific for the brainstem and identified that astrocytes were enriched
503 in the Sp5C. Astrocytes in different lamina of the spinal cord dorsal horn are known to have
504 specific functions, including modulation of nociception and facilitation of tactile information
505 [106]. Interestingly, the morphology of Sp5C astrocytes closely resembles the interlaminar
506 astrocytes present only in the primate outer cortices [107,108], or radial glial cells and, recent
507 evidence shows that brainstem/cortical astrocytes have proliferative/migratory potentials [45].
508 Increased reactive gliosis or hypertrophied nature of Gfap+ fibrous astrocytes in the mTBI and

509 the presence of Gfap mRNA in the end processes of these fibrous astrocytes in the Sp5C suggest
510 that these astrocytes are dynamically modulated in the brainstem long after injury. Similar results
511 in the Sp5C were reported in partial ligation of the infraorbital trigeminal nerve [37], where
512 elevated astrocytes persisted even months after injury [76]. Although morphology of GFAP+
513 astrocytes are different in the spinal dorsal horn compared to Sp5C [109], because of the close
514 proximity to Slc1a2, functionally, GFAP+ fibers in the Sp5C could modulate neurons via
515 glutamate signaling involved in neuropathic pain [45,110–113]. In line with this, astrogliosis in
516 the Sp5C has been shown to be involved in the development [114] and maintenance of pain
517 [115]. Although we have not tested long term characteristics of reactive gliosis, Sp5C astrocytes
518 may play a major role in the development of headache-like symptoms following mTBI and could
519 be a target of treatment in chronic pain [116].

520 **Potential involvement of inflammation in mTBI induced headache**

521 Due to the extensive damage caused by the acceleration mTBI model to the brainstem, it was
522 expected that injury related pathology might extend beyond Sp5C. Microglial proliferation was
523 more prominent in white matter tracts (spinocerebellar/tectospinal/pyramidal tracts) than in gray
524 matter areas. While the role of microglia in white matter tracts is suggested to involve
525 phagocytosis of degenerating axons, as seen in spinal cord injury [117], their function in gray
526 matter may differ. For instance, activated microglia in the gracile nucleus, associated with touch
527 and proprioception, might contribute to pain symptoms, as seen in preclinical studies linking TBI
528 to plantar tactile hypersensitivity [83]. Although we did not assess plantar tactile sensitivity in
529 this study, the presence of activated microglia in the gracile nucleus indicated a potential role for
530 inflammation in the paratrigeminal region.

531 Additionally, reactive astrogliosis in various brainstem regions, often in close proximity to
532 microglia, suggests potential astrocyte-microglia interactions influencing neuroinflammation and
533 pain modulation [51]. The increased expression of microglial markers in the Sp5C seven days
534 post-injury, combined with the extended reach of astrocytic fibers, hints at a possible recruitment
535 of astrocytes by microglia during neuroinflammation [118]. This interaction could potentially
536 modulate glutamate signaling in the Sp5C, given the proximity of astrocytic fibers to Slc1a2. The
537 widespread presence of Slc1a2 throughout the Sp5C [119], indicates ongoing glutamate
538 signaling in healthy mice for facial proprioception, suggesting that increased reactive astrocytes
539 in mTBI might further influence this signaling pathway. Consequently, the combined effects of
540 reactive astrocytosis and elevated microglia activation could potentially regulate pain within the
541 trigeminal system.

542 Since we observed increased inflammatory response in the Sp5C and its neighboring region in
543 the brainstem, we sought to elucidate underlying neural mechanisms of pain. Calretinin-positive
544 interneurons, a population known for their involvement in inflammation-induced pain [52],
545 increased in number and reorganize within the superficial laminae of the Sp5C following mild
546 TBI. This pattern closely resembles with those observed in the spinal dorsal horn after peripheral
547 nerve injury [120]. Calretinin interneurons have been implicated in the activation of ascending
548 pain signals via projections to the parabrachial nucleus leading to chronification of pain [121].
549 Considering the predominant excitatory nature of these interneurons and their role in pain
550 propagation [122,123], it is possible that reorganization from lamina II to lamina I and the
551 increase in the number of calretinin-ir neurons following mTBI may contribute to the enhanced
552 allodynia detected one week post-injury. Moreover, such recruitment would also explain an
553 increase in microglia and astrocytes in the lamina I of the Sp5C to further augment ascending

554 somatosensory pain signals. Further investigation into the interaction between glia and calretinin
555 interneurons is warranted.

556 **Conclusions**

557

558 Overall, mTBI in mice developed periorbital sensitivity and grimace days after injury thereby
559 exhibiting headache-like symptoms. While widespread inflammatory markers were observed in
560 several pain-related regions, transcriptomic analyses revealed that head injury induced distinct
561 pathogenic gene expression profiles in peripheral TG and central Sp5C, where glia have distinct
562 functional roles. Thus, glia in the trigeminal regions appear to modulate headache-like symptoms
563 and offer an avenue for further research on treatment targets for PTH following mTBI.

564 **Availability of Data and Materials**

565 The underlying data and computational scripts employed in this study will be shared upon
566 request. Mild TBI induced differentially expressed gene from each tissue region (TG, Sp5C and
567 PAG) are available in Additional file 3. Data from Yang et al., 2022 for custom gene sets used in
568 GSEA and meta-analysis can be found in GEO GSE197289 and data from Nguyen et al., 2019
569 used for comparison of injury models can be found in GEO GSE131272.

570 **Abbreviations**

571 mTBI - Mild traumatic brain injury

572 Sp5C - Trigeminal nucleus caudalis

573 TG - Trigeminal ganglion

574 PAG - Periaqueductal gray

575 IRt - Intermediate reticular nucleus

576 Mdv - Medullary reticular nucleus, ventral part

577 py - pyramidal tract

578 sc - spinocerebellar tract

579 ts - tectospinal tract

580 Iba1 - Ionized calcium binding adaptor molecule 1

581 CD68 - Cluster of differentiation 68

582 GSEA - Gene set enrichment analysis

583 CHIMERA - closed-head impact model of engineered rotational acceleration

584 Gapdh - Glyceraldehyde 3-phosphate dehydrogenase

585 Gfap - Glial fibrillary acidic protein

586 Gja1 - gap junction alpha-1

587 Egr1 - Early growth response factor 1

588 Aif1 - Allograft inflammatory factor 1

589 Kcnj10 - Potassium inwardly rectifying channel subfamily J member 10

590 Slc1a2 - solute carrier family 1 (glial high affinity glutamate transporter), member 2

591 ***Ethics approval and consent to participate***

592 All animal procedures were conducted in accordance with the Office for Laboratory Animal
593 Welfare (OLAW), National Institutes of Health (NIH) and American Veterinary Medical
594 Association (AVMA) Guidelines for the Euthanasia of Animals guidelines and approved by the
595 Uniformed Services University of the Health Sciences (USUHS) Institutional Animal Care and
596 Use Committee (IACUC).

597 ***Consent for publication***

598 Not applicable.

599 ***Competing interests***

600 The authors declare that they have no competing interests.

601 ***Funding Statement***

602 This work was supported by the Congressionally Directed Medical Research Programs
603 (CDMRP) award (W81XWH2120457).

604 ***Authors' contributions***

605 GN and YZ designed the experiments. GN conducted the experiments, analyzed the data and
606 wrote the manuscript. GN and YZ interpreted the data and revised the manuscript. Y.Z. acquired
607 the research funding. All authors have read and agreed to the submitted version of the
608 manuscript.

Acknowledgements

We would like to thank Jie Wen, MD, Ph.D., for performing the von Frey testing. We also thank Amanda Fu, MD, and Laura Tucker, MS at the USUHS Preclinical Behavior and Modeling Core for assistance with mouse procedures, Dennis McDaniel, Ph.D., and Fritz Lischka, Ph.D., at the USUHS Biomedical Instrumentation Core for Imaging, and Gemini for text editing. We gratefully acknowledge the Student Bioinformatics Initiative (SBI) at the USUHS for providing crucial high-performance computing resources. We also extend our thanks to Andrew Frank, MS, Clifton Dalgard, Ph.D., and Matthew Wilkerson, Ph.D., for their insightful discussions and feedback on our bioinformatics approaches.

Disclaimer

The statements and data presented in this manuscript belong to the authors of the manuscript and do not reflect the views of the Department of Defense or the Uniformed Services University of the Health Sciences.

631 **Figure Legends:**

632

633 **Fig 1. Behavioral assessment following mTBI in mice.** a) Schematic representation of the
634 experimental procedure involved in mTBI, with an illustration depicting the location of mTBI
635 hits in the dorsum of the head and a timeline depicting behavioral measurement and sample
636 collection. b) Increased righting reflex, a measure of comatose state, in mice following mTBI in
637 the bregma or pre-bregma locations. c) Depending on localization of injury, mTBI induced
638 differential peri-orbital sensitivity or mechanical threshold measured by von Frey filaments in
639 the periorbital region. d) Increased grimace score in mTBI mice observed 5 days after the last
640 mTBI. *, $p<0.05$, **, $p<0.01$, ***, $p<0.001$ and ****, $p<0.0001$. (n=5-6/group, Mean± SEM).

641 **Fig 2. Quantitative gene expression in TG and brain regions following mTBI in mice.** a)
642 Fold change (qPCR) in Egr1 (early growth response 1) mRNA expression in the TG of mTBI
643 mice after 7 days following hits in different positions of the head. Data (n=6) in the bar graph are
644 represented as mean ± standard error. *, $p<0.05$. b) Heatmap representing qPCR fold changes
645 (FC) in the gene expression of Gfap, Aif1, Cd68 and Trem2 in the Sp5C, PAG, PB/LC and the
646 thalamus of mTBI mice with hits in both bregma and pre-bregma positions. *, $p<0.05$, **,
647 $p<0.01$ (n=5-6/group).

648 **Fig 3. Transcriptome analyses from TG, Sp5C and PAG following mTBI**. a) Principal
649 component analysis of mouse transcriptome from TG, Sp5C, and PAG shows three distinct gene
650 clusters belonging to the peripheral ganglion (TG), the medulla (Sp5C) and midbrain (PAG)
651 regions. b) Dot plots of Gene Set Enrichment Analysis (GSEA) in the TG following repetitive
652 mTBI, representing the 15 most differentially enriched biological process gene sets obtained
653 from the C5 collection in the mouse molecular signatures database. Dot plots of GSEA analysis
654 in the Sp5C (c) and PAG (d) of mTBI mice, representing the 20 and 30, respectively, most

655 differentially enriched biological process gene sets obtained from the C5 collection in the mouse
656 molecular signatures database. Data used for PCA and GSEA were obtained from
657 n=3/group/region.

658 **Fig. 4. Comparison of the TG transcriptome of mTBI mice with TG cell atlas.** a) Dot plot
659 representing enriched gene clusters of different cell types in the TG. Non-neuronal gene clusters
660 have positively normalized enrichment scores (p-adjusted values <0.2) and neuronal gene
661 clusters have a negative normalized enrichment score (p-adjusted <0.05). Abbreviations:
662 cLTMRs - C-fiber low threshold mechanoreceptor (LTMR); fibroblast_Dcn - DCN+ meningeal
663 fibroblasts; fibroblast_Mgp - MGP+ meningeal fibroblast; NF1, neurofilament+ A-LTMR
664 enriched for A-beta-field; NF2, neurofilament+ A-LTMR enriched for A-beta-RA and A-beta-
665 field; NF3, neurofilament+ LTMR enriched for A-delta; NP - non-peptidergic nociceptor;
666 Schwann_M, myelinating Schwann cells; SST, somatostatin positive pruriceptors.

667 **Fig. 5. Mild TBI induced gene expression of satellite glial markers in the TG.** a) Fold change
668 (qPCR) in gene expression of satellite glial markers (Gfap, Gja1 and Slc1a2) in the TG of mTBI
669 mice. Bar graphs show mRNA expression on day 1 and day 8 after the last mTBI. Data (n=5-
670 6/group) in the bar graph are represented as mean±standard error. *, p<0.05, **, p<0.01. b)
671 Localization of mRNA expression of Kcnj10 (green), Gfap (red) and Slc1a2 (magenta) in the TG
672 of sham and mTBI mice obtained at 7 days post injury. Scale bar = 50µm.

673 **Fig. 6. Distinct patterns of inflammatory markers in the trigeminocervical complex of**
674 **mTBI mice.** a) A representative image of CD68+, Iba1+ cells in caudal Sp5C (AP coordinate ~ -
675 8.6) from sham and mTBI mice. b) A representative image of CD68+, Iba1+ cells at the level of
676 trigeminal region (Bregma coordinate ~-8.1) from a sham and mTBI mouse. c) Increased
677 CD68/Iba1+ cell count, most notable in the fiber tracts and in the gracile nucleus of mTBI mice.

678 d) Increased CD68 intensity within Iba1+ cells in the Sp5C of mTBI mice compared to the sham
679 group. n=10-15 cells/section; n=3 mice /group. Abbreviations: Cu - cuneate nucleus; Gr -
680 gracile nucleus; IRt - Intermediate reticular nucleus; Mdv - Medullary reticular nucleus, ventral
681 part; py - pyramidal tract; sc - spinocerebellar tract; Sp5c (MDH) - spinal trigeminal nucleus
682 caudalis (medullary dorsal horn); ts - tectospinal tract. *, $p<0.05$, **, $p<0.01$, ***, $p<0.001$ and
683 ****, $p<0.0001$. (n=5-6/group, Mean± SEM).

684 **Fig. 7. Reactive astrogliosis in brainstem of mTBI mice 7 days following injury**. a) An
685 example brainstem section at the Bregma level -8.2 stained with GFAP (green,
686 immunohistochemistry) and Gfap (red, in situ hybridization). Scale bar = 200 µm. b) Insets in
687 Fig 7a representing differences in Gfap mRNA/GFAP antibody (Ab) staining in various
688 brainstem regions. Representative confocal images from a sham (c) and a mTBI (d) mouse
689 showing colocalization of Gfap mRNA (red, in situ hybridization) on GFAP+ astrocytes (green,
690 immunohistochemistry) in the Sp5c. Scale bar = 50 µm. Inset of 7d mTBI mice shows increased
691 Gfap mRNA expression in the processes of GFAP+ astrocytes in lamina III of Sp5C. Scale bar =
692 20 µm. e) Graph representing percent of Gfap mRNA in GFAP+ fibrous astrocytes in the Sp5c
693 between sham (n=155 fibers) and mTBI (n=168 fibers) group. f) Close proximity of GFAP-ir
694 fibers or cells to Iba1/CD68+ cells in different regions of the brainstem are shown in white
695 arrows. GFAP-ir fibers or cells that are not in close contact with Iba1/CD68+ cells are shown in
696 purple arrows. g) Representative image showing localized expression of Slc1a2 in the Sp5C of a
697 sham and mTBI mouse. Scale bar = 500µm. h) Presence of GFAP+ astrocytes (green,
698 immunohistochemistry) in close proximity to Slc1a2 mRNA puncta (purple, in situ
699 hybridization) in the lamina III of Sp5C are shown in white arrows. Scale bar = 50 µm. IRt -
700 Intermediate reticular nucleus; Mdv - Medullary reticular nucleus, ventral part; py - pyramidal

701 tract; sc - spinocerebellar tract; Sp5c (MDH)- spinal trigeminal nucleus caudalis (medullary
702 dorsal horn); ts - tectospinal tract.

703 **Fig. 8. Calretinin in the Sp5C of mTBI mice potentially involved in trigeminal pain.** a)
704 Reorganization of calretinin-ir was observed from outer lamina II to lamina I of mTBI mice
705 (n=3; Bregma coordinate ~8.2). Full extent of this reorganization is shown in Additional File 7.
706 b) Representative images from a sham and mTBI mice at Sp5C showing the shift in calretinin-ir
707 from lamina II to lamina I. Scale bar = 50 µm. c) Increased number of calretinin-ir neurons in the
708 rostral Sp5c compared to the caudal Sp5c of mTBI mice. **, $p<0.01$.

709

710
711 **Additional Files**

712 **Additional File1**. Righting reflex in each of four mTBI days (n=6/group).

713 **Additional File 2**. Bar graphs representing grimace at 6, 16- and 22-days post mTBI (dpi) in
714 bregma position (n=4-5/group).

715 **Additional File 3.** Enriched Go terms and differentially expressed genes from three different
716 regions (TG, Sp5C and PAG) following mTBI.

717 **Additional File 4**. Dot plot representing astrocyte specific enriched gene sets in the Sp5C
718 following mTBI.

719 **Additional File 5**. Distinct expression pattern of CD68+, Iba1+ cells in the brainstem. Fiber
720 tracts, specifically spinocerebellar tract (sc), show a distinct morphological profile compared to
721 the microglia in the gray matter (Sp5C, Gr, Mdv). Gr - gracile nucleus; Mdv - Medullary
722 reticular nucleus.

723 **Additional File 6**. Increased presence of GFAP+ fibrous astrocytes in the Sp5C compared to the

724 paratrigeminal regions. Rare appearance of protoplasmic astrocytes in the Sp5C and prominent
725 protoplasmic appears in the reticular formation in both Sham and mTBI. IRt - Intermediate
726 reticular nucleus.

727 **Additional File 7.** Representative images from sham and mTBI mice showing calretinin-ir
728 neurons in the lamina I of Sp5C. Dotted white lines represent the Ib4+ staining. Atlas plate at the
729 level of ~ -8.3 from bregma. Scale bar = 200 µm.

730 **References:**

731 1. Peskind ER, Brody D, Cernak I, McKee A, Ruff RL. Military- and sports-related mild
732 traumatic brain injury: clinical presentation, management, and long-term consequences. J Clin
733 Psychiatry. 2013;74:180–8; quiz 188.

734 2. Ashina H, Eigenbrodt AK, Seifert T, Sinclair AJ, Scher AI, Schytz HW, et al. Post-traumatic
735 headache attributed to traumatic brain injury: classification, clinical characteristics, and
736 treatment. Lancet Neurol. 2021;20:460–9.

737 3. Couch JR, Bearss C. Chronic daily headache in the posttrauma syndrome: relation to extent of
738 head injury. Headache. 2001;41:559–64.

739 4. Holtkamp MD, Grimes J, Ling G. Concussion in the Military: an Evidence-Base Review of
740 mTBI in US Military Personnel Focused on Posttraumatic Headache. Curr Pain Headache Rep.
741 2016;20:37.

742 5. Stovner LJ, Schrader H, Couch JR Jr, Lipton RB, Stewart WF, Scher AI. Head or neck injury
743 increases the risk of chronic daily headache: a population-based study. Neurology. 2008. p. 383–
744 5.

745 6. Couch JR, Lipton RB, Stewart WF, Scher AI. Head or neck injury increases the risk of chronic
746 daily headache: a population-based study. Neurology. 2007;69:1169–77.

747 7. Theeler BJ, Flynn FG, Erickson JC. Chronic daily headache in U.S. soldiers after concussion.
748 Headache. 2012;52:732–8.

749 8. Nampiaparampil DE. Prevalence of chronic pain after traumatic brain injury: a systematic
750 review. JAMA. 2008;300:711–9.

751 9. Cohen SP, Plunkett AR, Wilkinson I, Nguyen C, Kurihara C, Flagg A 2nd, et al. Headaches
752 during war: analysis of presentation, treatment, and factors associated with outcome.
753 Cephalalgia. 2012;32:94–108.

754 10. Finkel AG, Yerry JA, Klaric JS, Ivins BJ, Scher A, Choi YS. Headache in military service
755 members with a history of mild traumatic brain injury: A cohort study of diagnosis and
756 classification. Cephalalgia. 2017;37:548–59.

757 11. Hoge CW, McGurk D, Thomas JL, Cox AL, Engel CC, Castro CA. Mild traumatic brain
758 injury in U.S. Soldiers returning from Iraq. N Engl J Med. 2008;358:453–63.

759 12. Irvine K-A, Clark JD. Chronic Pain After Traumatic Brain Injury: Pathophysiology and Pain
760 Mechanisms. Pain Med. 2017;19:1315–33.

761 13. Basbaum AI, Fields HL. Endogenous pain control systems: brainstem spinal pathways and
762 endorphin circuitry. Annu Rev Neurosci. 1984;7:309–38.

763 14. Woolf CJ. Central sensitization: implications for the diagnosis and treatment of pain. Pain.
764 2011;152:S2–15.

765 15. Dodick D, Silberstein S. Central sensitization theory of migraine: clinical implications.
766 Headache. 2006;46 Suppl 4:S182–91.

767 16. Vila-Pueyo M, Hoffmann J, Romero-Reyes M, Akerman S. Brain structure and function
768 related to headache: Brainstem structure and function in headache. Cephalalgia. 2019;39:1635–
769 60.

770 17. Terrier L-M, Hadjikhani N, Velut S, Magnain C, Amelot A, Bernard F, et al. The trigeminal
771 system: The meningovascular complex- A review. J Anat. 2021;239:1–11.

772 18. Kuramoto E, Fukushima M, Sendo R, Ohno S, Iwai H, Yamanaka A, et al. Three-
773 dimensional topography of rat trigeminal ganglion neurons using a combination of retrograde
774 labeling and tissue-clearing techniques. J Comp Neurol. 2024;532:e25584.

775 19. Capra NF, Dessem D. Central connections of trigeminal primary afferent neurons:
776 topographical and functional considerations. Crit Rev Oral Biol Med. 1992;4:1–52.

777 20. Hanani M, Spray DC. Emerging importance of satellite glia in nervous system function and
778 dysfunction. Nat Rev Neurosci. 2020;21:485–98.

779 21. McGinnis A, Ji R-R. The Similar and Distinct Roles of Satellite Glial Cells and Spinal
780 Astrocytes in Neuropathic Pain. Cells [Internet]. 2023;12. Available from:
781 http://dx.doi.org/10.3390/cells12060965

782 22. Gennarelli TA, Thibault LE, Adams JH, Graham DI, Thompson CJ, Marcincin RP. Diffuse
783 axonal injury and traumatic coma in the primate. Ann Neurol. 1982;12:564–74.

784 23. Meaney DF, Morrison B, Dale Bass C. The mechanics of traumatic brain injury: a review of
785 what we know and what we need to know for reducing its societal burden. J Biomech Eng.
786 2014;136:021008.

787 24. Burstein R, Yamamura H, Malick A, Strassman AM. Chemical stimulation of the intracranial

788 dura induces enhanced responses to facial stimulation in brain stem trigeminal neurons. J
789 Neurophysiol. 1998;79:964–82.

790 25. Noseda R, Burstein R. Migraine pathophysiology: anatomy of the trigeminovascular pathway
791 and associated neurological symptoms, CSD, sensitization and modulation of pain. Pain
792 [Internet]. 2013;154 Suppl 1. Available from: https://journals.lww.com/00006396-201312001-
793 00005

794 26. Iwata K, Miyachi S, Imanishi M, Tsuboi Y, Kitagawa J, Teramoto K, et al. Ascending
795 multisynaptic pathways from the trigeminal ganglion to the anterior cingulate cortex. Exp
796 Neurol. 2011;227:69–78.

797 27. Goadsby PJ, Holland PR, Martins-Oliveira M, Hoffmann J, Schankin C, Akerman S.
798 Pathophysiology of Migraine: A Disorder of Sensory Processing. Physiol Rev. 2017;97:553–
799 622.

800 28. Shinoda M, Kubo A, Hayashi Y, Iwata K. Peripheral and Central Mechanisms of Persistent
801 Orofacial Pain. Front Neurosci. 2019;13:1227.

802 29. Lighthall JW, Dixon CE, Anderson TE. Experimental models of brain injury. J Neurotrauma.
803 1989;6:83–97.

804 30. Nilsson B, Pontén U, Voigt G. Experimental head injury in the rat. Part 1: Mechanics,
805 pathophysiology, and morphology in an impact acceleration trauma model. J Neurosurg.
806 1977;47:241–51.

807 31. Gurdjian ES, Lissner HR, Webster JE, Latimer FR, Haddad BF. Studies on experimental
808 concussion: relation of physiologic effect to time duration of intracranial pressure increase at
809 impact. Neurology. 1954;4:674–81.

810 32. Cernak I. Animal models of head trauma. NeuroRx. 2005;2:410–22.

811 33. Xiong Y, Mahmood A, Chopp M. Animal models of traumatic brain injury. Nat Rev
812 Neurosci. 2013;14:128–42.

813 34. Hoogenboom WS, Branch CA, Lipton ML. Animal models of closed-skull, repetitive mild
814 traumatic brain injury. Pharmacol Ther. 2019;198:109–22.

815 35. Nguyen MQ, Le Pichon CE, Ryba N. Stereotyped transcriptomic transformation of
816 somatosensory neurons in response to injury. Elife [Internet]. 2019;8. Available from:
817 http://dx.doi.org/10.7554/eLife.49679

818 36. Yang L, Xu M, Bhuiyan SA, Li J, Zhao J, Cohrs RJ, et al. Human and mouse trigeminal
819 ganglia cell atlas implicates multiple cell types in migraine. Neuron. 2022;110:1806–21.e8.

820 37. Xu M, Aita M, Chavkin C. Partial infraorbital nerve ligation as a model of trigeminal nerve
821 injury in the mouse: behavioral, neural, and glial reactions. J Pain. 2008;9:1036–48.

822 38. Namjoshi DR, Cheng WH, McInnes KA, Martens KM, Carr M, Wilkinson A, et al. Merging
823 pathology with biomechanics using CHIMERA (Closed-Head Impact Model of Engineered
824 Rotational Acceleration): a novel, surgery-free model of traumatic brain injury. Mol
825 Neurodegener. 2014;9:1–18.

826 39. Smith DH, Nonaka M, Miller R, Leoni M, Chen XH, Alsop D, et al. Immediate coma
827 following inertial brain injury dependent on axonal damage in the brainstem. J Neurosurg.
828 2000;93:315–22.

829 40. Langford DJ, Bailey AL, Chanda ML, Clarke SE, Drummond TE, Echols S, et al. Coding of
830 facial expressions of pain in the laboratory mouse. Nat Methods. 2010;7:447–9.

831 41. Zhu A, Ibrahim JG, Love MI. Heavy-tailed prior distributions for sequence count data:
832 removing the noise and preserving large differences. Bioinformatics. 2019;35:2084–92.

833 42. Wickham H, Averick M, Bryan J, Chang W, McGowan L, François R, et al. Welcome to the
834 tidyverse. J Open Source Softw. 2019;4:1686.

835 43. Mamet J, Klukinov M, Yaksh TL, Malkmus SA, Williams S, Harris S, et al. Single
836 intrathecal administration of the transcription factor decoy AYX1 prevents acute and chronic
837 pain after incisional, inflammatory, or neuropathic injury. Pain. 2014;155:322.

838 44. Bereiter DA, Hirata H, Hu JW. Trigeminal subnucleus caudalis: beyond homologies with the
839 spinal dorsal horn. Pain. 2000;88:221–4.

840 45. John Lin C-C, Yu K, Hatcher A, Huang T-W, Lee HK, Carlson J, et al. Identification of
841 diverse astrocyte populations and their malignant analogs. Nat Neurosci. 2017;20:396–405.

842 46. Jacquin MF, Semba K, Rhoades RW, Egger MD. Trigeminal primary afferents project
843 bilaterally to dorsal horn and ipsilaterally to cerebellum, reticular formation, and cuneate,
844 solitary, supratrigeminal and vagal nuclei. Brain Res. 1982;246:285–91.

845 47. Jacquin MF, Chiaia NL, Rhoades RW. Trigeminal projections to contralateral dorsal horn:
846 central extent, peripheral origins, and plasticity. Somatosens Mot Res. 1990;7:153–83.

847 48. Voisin DL, Doméjean-Orliaguet S, Chalus M, Dallel R, Woda A. Ascending connections
848 from the caudal part to the oral part of the spinal trigeminal nucleus in the rat. Neuroscience.
849 2002;109:183–93.

850 49. Sofroniew MV. Astrocyte barriers to neurotoxic inflammation. Nat Rev Neurosci.
851 2015;16:249–63.

852 50. Hasel P, Rose IVL, Sadick JS, Kim RD, Liddelow SA. Neuroinflammatory astrocyte
853 subtypes in the mouse brain. Nat Neurosci. 2021;24:1475–87.

854 51. Linnerbauer M, Wheeler MA, Quintana FJ. Astrocyte Crosstalk in CNS Inflammation.
855 Neuron. 2020;108:608–22.

856 52. Peirs C, Williams S-PG, Zhao X, Arokiaraj CM, Ferreira DW, Noh M-C, et al. Mechanical
857 Allodynia Circuitry in the Dorsal Horn Is Defined by the Nature of the Injury. Neuron.
858 2021;109:73–90.e7.

859 53. Ommaya AK, Gennarelli TA. Cerebral concussion and traumatic unconsciousness.
860 Correlation of experimental and clinical observations of blunt head injuries. Brain. 1974;97:633–
861 54.

862 54. Cifu D, Hurley R, Peterson M, Cornis-Pop M, Rikli PA, Ruff RL, et al. Clinical practice
863 guideline: Management of Concussion/Mild Traumatic Brain Injury. J Rehabil Res Dev.
864 2009;46:CP1.

865 55. Headache Classification Committee of the International Headache Society (IHS) The
866 International Classification of Headache Disorders, 3rd edition. Cephalalgia. 2018;38:1–211.

867 56. Ruff RM, Iverson GL, Barth JT, Bush SS, Broshek DK, NAN Policy and Planning
868 Committee. Recommendations for diagnosing a mild traumatic brain injury: a National Academy
869 of Neuropsychology education paper. Arch Clin Neuropsychol. 2009;24:3–10.

870 57. Mercer Lindsay N, Chen C, Gilam G, Mackey S, Scherrer G. Brain circuits for pain and its
871 treatment. Sci Transl Med. 2021;13:eabj7360.

872 58. Basbaum AI, Bautista DM, Scherrer G, Julius D. Cellular and molecular mechanisms of pain.
873 Cell. 2009;139:267–84.

874 59. Theeler BJ, Erickson JC. Mild head trauma and chronic headaches in returning US soldiers.
875 Headache. 2009;49:529–34.

876 60. Laurer HL, Bareyre FM, Lee VMY, Trojanowski JQ, Longhi L, Hoover R, et al. Mild head
877 injury increasing the brain's vulnerability to a second concussive impact. J Neurosurg.
878 2001;95:859–70.

879 61. Defrin R, Gruener H, Schreiber S, Pick CG. Quantitative somatosensory testing of subjects
880 with chronic post-traumatic headache: implications on its mechanisms. Eur J Pain. 2010;14:924–
881 31.

882 62. Defrin R, Riabinin M, Feingold Y, Schreiber S, Pick CG. Deficient pain modulatory systems
883 in patients with mild traumatic brain and chronic post-traumatic headache: implications for its
884 mechanism. J Neurotrauma. 2015;32:28–37.

885 63. Gracely RH, Lynch SA, Bennett GJ. Painful neuropathy: altered central processing
886 maintained dynamically by peripheral input. Pain. 1992;51:175–94.

887 64. Burstein R. Deconstructing migraine headache into peripheral and central sensitization. Pain.
888 2001;89:107–10.

889 65. Goadsby PJ, Hoskin KL. The distribution of trigeminovascular afferents in the nonhuman
890 primate brain Macaca nemestrina: a c-fos immunocytochemical study. J Anat. 1997;190 (Pt

3):367–75.

66. Hoffman JM, Lucas S, Dikmen S, Braden CA, Brown AW, Brunner R, et al. Natural history of headache after traumatic brain injury. J Neurotrauma. 2011;28:1719–25.

67. Buse DC, Greisman JD, Baigi K, Lipton RB. Migraine Progression: A Systematic Review. An Editorial Comment. Headache. 2019;59:974–6.

68. Dubner R, Ren K. Brainstem mechanisms of persistent pain following injury. J Orofac Pain. 2004;18:299–305.

69. Rodriguez E, Sakurai K, Xu J, Chen Y, Toda K, Zhao S, et al. A craniofacial-specific monosynaptic circuit enables heightened affective pain. Nat Neurosci. 2017;20:1734–43.

70. Cechetto DF, Standaert DG, Saper CB. Spinal and trigeminal dorsal horn projections to the parabrachial nucleus in the rat. J Comp Neurol. 1985;240:153–60.

71. Mantyh PW. The ascending input to the midbrain periaqueductal gray of the primate. J Comp Neurol. 1982;211:50–64.

72. Wiberg M, Westman J, Blomqvist A. The projection to the mesencephalon from the sensory trigeminal nuclei. An anatomical study in the cat. Brain Res. 1986;399:51–68.

73. Liu Y, Broman J, Zhang M, Edvinsson L. Brainstem and thalamic projections from a craniovascular sensory nervous centre in the rostral cervical spinal dorsal horn of rats. Cephalalgia. 2009;29:935–48.

74. Gauriau C, Bernard J-F. A comparative reappraisal of projections from the superficial laminae of the dorsal horn in the rat: the forebrain. J Comp Neurol. 2004;468:24–56.

75. Witcher KG, Dziabis JE, Bray CE, Gordillo AJ, Kumar JE, Eiferman DS, et al. Comparison between midline and lateral fluid percussion injury in mice reveals prolonged but divergent cortical neuroinflammation. Brain Res. 2020;1746:146987.

76. Carbonell WS, Grady MS. Regional and temporal characterization of neuronal, glial, and axonal response after traumatic brain injury in the mouse. Acta Neuropathol. 1999;98:396–406.

77. McIntosh TK, Smith DH, Meaney DF, Kotapka MJ, Gennarelli TA, Graham DI. Neuropathological sequelae of traumatic brain injury: relationship to neurochemical and biomechanical mechanisms. Lab Invest. 1996;74:315–42.

78. Tse KM, Tan LB, Lee SJ, Lim SP, Lee HP. Investigation of the relationship between facial injuries and traumatic brain injuries using a realistic subject-specific finite element head model. Accid Anal Prev. 2015;79:13–32.

79. Brommer B, Engel O, Kopp MA, Watzlawick R, Müller S, Prüss H, et al. Spinal cord injury-induced immune deficiency syndrome enhances infection susceptibility dependent on lesion level. Brain. 2016;139:692–707.

925 80. Yang L, Xu M, Bhuiyan SA, Li J, Zhao J, Cohrs RJ, et al. Human and mouse trigeminal
926 ganglia cell atlas implicates multiple cell types in migraine. Neuron. 2022;110:1806–21.e8.

927 81. Devor M, Amir R, Rappaport ZH. Pathophysiology of trigeminal neuralgia: the ignition
928 hypothesis. Clin J Pain. 2002;18:4–13.

929 82. Pradhan AA, Smith ML, McGuire B, Tarash I, Evans CJ, Charles A. Characterization of a
930 novel model of chronic migraine. Pain. 2014;155:269–74.

931 83. Wattiez A-S, Castonguay WC, Gaul OJ, Waite JS, Schmidt CM, Reis AS, et al. Different
932 forms of traumatic brain injuries cause different tactile hypersensitivity profiles. Pain.
933 2021;162:1163–75.

934 84. Wen J, Tanaka M, Zhang Y. Inhibition of 2-AG hydrolysis alleviates posttraumatic headache
935 attributed to mild traumatic brain injury. J Headache Pain. 2024;25:115.

936 85. Bree D, Levy D. Development of CGRP-dependent pain and headache related behaviours in
937 a rat model of concussion: Implications for mechanisms of post-traumatic headache.
938 Cephalalgia. 2018;38:246–58.

939 86. Guo Z, Czerpaniak K, Zhang J, Cao Y-Q. Increase in trigeminal ganglion neurons that
940 respond to both calcitonin gene-related peptide and pituitary adenylate cyclase-activating
941 polypeptide in mouse models of chronic migraine and posttraumatic headache. Pain.
942 2021;162:1483–99.

943 87. Tang-Schomer MD, Patel AR, Baas PW, Smith DH. Mechanical breaking of microtubules in
944 axons during dynamic stretch injury underlies delayed elasticity, microtubule disassembly, and
945 axon degeneration. FASEB J. 2010;24:1401–10.

946 88. Blennow K, Hardy J, Zetterberg H. The neuropathology and neurobiology of traumatic brain
947 injury. Neuron. 2012;76:886–99.

948 89. Aita M, Byers MR, Chavkin C, Xu M. Trigeminal injury causes kappa opioid-dependent
949 allodynic, glial and immune cell responses in mice. Mol Pain. 2010;6:8.

950 90. Liu L, Rudin M, Kozlova EN. Glial cell proliferation in the spinal cord after dorsal
951 rhizotomy or sciatic nerve transection in the adult rat. Exp Brain Res. 2000;131:64–73.

952 91. Mapps AA, Thomsen MB, Boehm E, Zhao H, Hattar S, Kuruvilla R. Diversity of satellite
953 glia in sympathetic and sensory ganglia. Cell Rep. 2022;38:110328.

954 92. Ji R-R, Donnelly CR, Nedergaard M. Astrocytes in chronic pain and itch. Nat Rev Neurosci.
955 2019;20:667–85.

956 93. Avraham O, Deng P-Y, Jones S, Kuruvilla R, Semenkovich CF, Klyachko VA, et al. Satellite
957 glial cells promote regenerative growth in sensory neurons. Nat Commun. 2020;11:1–17.

958 94. Vit J-P, Ohara PT, Bhargava A, Kelley K, Jasmin L. Silencing the Kir4.1 potassium channel

959 subunit in satellite glial cells of the rat trigeminal ganglion results in pain-like behavior in the
960 absence of nerve injury. J Neurosci. 2008;28:4161–71.

961 95. Zhang H, Mei X, Zhang P, Ma C, White FA, Donnelly DF, et al. Altered functional
962 properties of satellite glial cells in compressed spinal ganglia. Glia. 2009;57:1588–99.

963 96. Takeda M, Takahashi M, Nasu M, Matsumoto S. Peripheral inflammation suppresses inward
964 rectifying potassium currents of satellite glial cells in the trigeminal ganglia. Pain.
965 2011;152:2147–56.

966 97. Tsantoulas C, McMahon SB. Opening paths to novel analgesics: the role of potassium
967 channels in chronic pain. Trends Neurosci. 2014;37:146–58.

968 98. Butt AM, Kalsi A. Inwardly rectifying potassium channels (Kir) in central nervous system
969 glia: a special role for Kir4.1 in glial functions. J Cell Mol Med. 2006;10:33–44.

970 99. Ohara PT, Vit J-P, Bhargava A, Romero M, Sundberg C, Charles AC, et al. Gliopathic pain:
971 when satellite glial cells go bad. Neuroscientist. 2009;15:450–63.

972 100. Tang X, Schmidt TM, Perez-Leighton CE, Kofuji P. Inwardly rectifying potassium channel
973 Kir4.1 is responsible for the native inward potassium conductance of satellite glial cells in
974 sensory ganglia. Neuroscience. 2010;166:397–407.

975 101. Kung L-H, Gong K, Adedoyin M, Ng J, Bhargava A, Ohara PT, et al. Evidence for
976 glutamate as a neuroglial transmitter within sensory ganglia. PLoS One. 2013;8:e68312.

977 102. Satellite glial cells in sensory ganglia: its role in pain. Brazilian Journal of Anesthesiology
978 (English Edition). 2015;65:73–81.

979 103. Emsley JG, Macklis JD. Astroglial heterogeneity closely reflects the neuronal-defined
980 anatomy of the adult murine CNS. Neuron Glia Biol. 2006;2:175–86.

981 104. Oberheim NA, Goldman SA, Nedergaard M. Heterogeneity of Astrocytic Form and
982 Function. Astrocytes. 2012;23–45.

983 105. Verkhratsky A, Nedergaard M. Physiology of Astroglia. Physiol Rev. 2018;98:239–389.

984 106. Kronschläger MT, Siegert ASM, Resch FJ, Rajendran PS, Khakh BS, Sandkühler J.
985 Lamina-specific properties of spinal astrocytes. Glia. 2021;69:1749–66.

986 107. Andriezen WL. The Neuroglia Elements in the Human Brain. Br Med J. 1893;2:227–30.

987 108. Colombo JA, Yáñez A, Puissant V, Lipina S. Long, interlaminar astroglial cell processes in
988 the cortex of adult monkeys. J Neurosci Res. 1995;40:551–6.

989 109. Garrison CJ, Dougherty PM, Kajander KC, Carlton SM. Staining of glial fibrillary acidic
990 protein (GFAP) in lumbar spinal cord increases following a sciatic nerve constriction injury.
991 Brain Res. 1991;565:1–7.

992 110. Araque A, Carmignoto G, Haydon PG, Oliet SHR, Robitaille R, Volterra A.
993 Gliotransmitters travel in time and space. Neuron. 2014;81:728–39.

994 111. Nie H, Zhang H, Weng H-R. Bidirectional neuron-glia interactions triggered by deficiency
995 of glutamate uptake at spinal sensory synapses. J Neurophysiol. 2010;104:713–25.

996 112. Bardoni R, Ghirri A, Zonta M, Betelli C, Vitale G, Ruggieri V, et al. Glutamate-mediated
997 astrocyte-to-neuron signalling in the rat dorsal horn. J Physiol. 2010;588:831–46.

998 113. Anderson CM, Swanson RA. Astrocyte glutamate transport: review of properties,
999 regulation, and physiological functions. Glia. 2000;32:1–14.

1000 114. Colburn RW, Rickman AJ, DeLeo JA. The effect of site and type of nerve injury on spinal
1001 glial activation and neuropathic pain behavior. Exp Neurol. 1999;157:289–304.

1002 115. Okada-Ogawa A, Suzuki I, Sessle BJ, Chiang C-Y, Salter MW, Dostrovsky JO, et al.
1003 Astroglia in Medullary Dorsal Horn (Trigeminal Spinal Subnucleus Caudalis) Are Involved in
1004 Trigeminal Neuropathic Pain Mechanisms. J Neurosci. 2009;29:11161–71.

1005 116. Ji R-R, Xu Z-Z, Gao Y-J. Emerging targets in neuroinflammation-driven chronic pain. Nat
1006 Rev Drug Discov. 2014;13:533–48.

1007 117. Matson KJE, Russ DE, Kathe C, Hua I, Maric D, Ding Y, et al. Single cell atlas of spinal
1008 cord injury in mice reveals a pro-regenerative signature in spinocerebellar neurons. Nat
1009 Commun. 2022;13:5628.

1010 118. Liddelow SA, Guttenplan KA, Clarke LE, Bennett FC, Bohlen CJ, Schirmer L, et al.
1011 Neurotoxic reactive astrocytes are induced by activated microglia. Nature. 2017;541:481–7.

1012 119. Rothstein JD, Martin L, Levey AI, Dykes-Hoberg M, Jin L, Wu D, et al. Localization of
1013 neuronal and glial glutamate transporters. Neuron. 1994;13:713–25.

1014 120. Latremoliere A, Woolf CJ. Central sensitization: a generator of pain hypersensitivity by
1015 central neural plasticity. J Pain. 2009;10:895–926.

1016 121. Petitjean H, Bourojeni FB, Tsao D, Davidova A, Sotocinal SG, Mogil JS, et al. Recruitment
1017 of Spinoparabrachial Neurons by Dorsal Horn Calretinin Neurons. Cell Rep. 2019;28:1429–
1018 38.e4.

1019 122. Smith KM, Boyle KA, Madden JF, Dickinson SA, Jobling P, Callister RJ, et al. Functional
1020 heterogeneity of calretinin-expressing neurons in the mouse superficial dorsal horn: implications
1021 for spinal pain processing. J Physiol. 2015;593:4319–39.

1022 123. Smith KM, Browne TJ, Davis OC, Coyle A, Boyle KA, Watanabe M, et al. Calretinin
1023 positive neurons form an excitatory amplifier network in the spinal cord dorsal horn. Elife
1024 [Internet]. 2019;8. Available from: http://dx.doi.org/10.7554/eLife.49190

1025 124. Chaplan SR, Bach FW, Pogrel JW, et al (1994) Quantitative assessment of tactile allodynia

1026 in the rat paw. J Neurosci Methods 53:55–63

1027 125. Bonin RP, Bories C, De Koninck Y (2014) A simplified up-down method (SUDO) for
1028 measuring mechanical nociception in rodents using von Frey filaments. Mol Pain 10:26

1029 126. Kleczkowska P, Lipkowski AW. (2013) Neurotensin and neurotensin receptors:
1030 Characteristic, structure–activity relationship and pain modulation — A review. Eur J Pharmacol
1031 716:54–60

1032 127. Cox HC, Lea RA, Bellis C, et al (2011) Variants in the human potassium channel gene
1033 (KCNN3) are associated with migraine in a high risk genetic isolate. J Headache Pain 12:603–
1034 608

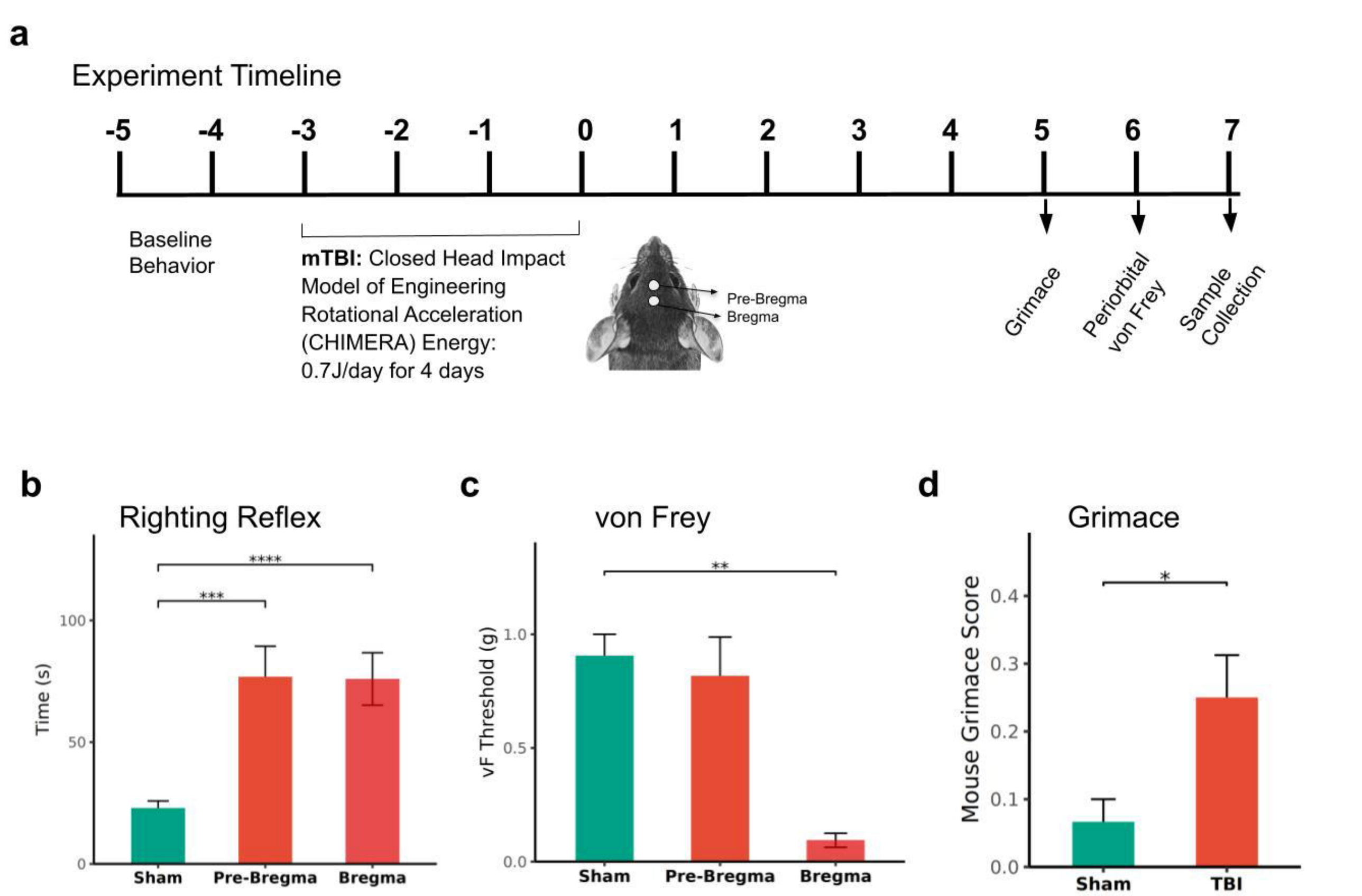
a
Experiment Timeline
-5
-4
-3
-2
-1
0
1
2
3
4
5
6
7
Baseline Behavior
mTBI: Closed Head Impact Model of Engineering Rotational Acceleration (CHIMERA) Energy: 0.7J/day for 4 days
Pre-Bregma
Bregma
Grimace
Periorbital von Frey
Sample Collection
b
Righting Reflex
****
***
Time (s)
100
50
0
Sham
Pre-Bregma
Bregma
c
von Frey
**
vF Threshold (g)
1.0
0.5
0.0
Sham
Pre-Bregma
Bregma
d
Grimace
*
Mouse Grimace Score
0.4
0.3
0.2
0.1
0.0
Sham
TBI

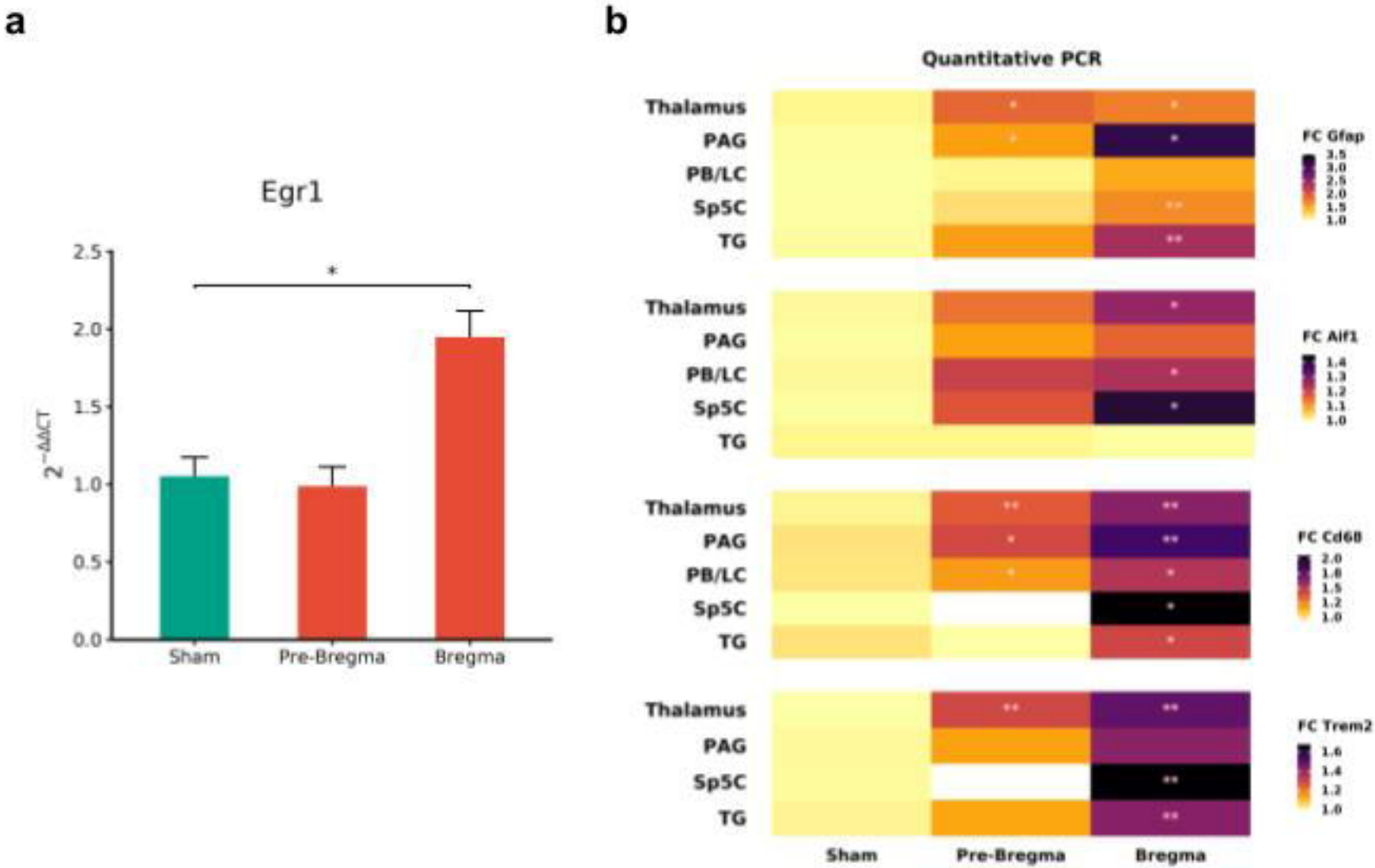
a
Egr1
2.5
2.0
1.5
1.0
0.5
0.0
$2^{-\Delta\Delta CT}$
*
Sham
Pre-Bregma
Bregma
b
Quantitative PCR
Thalamus
PAG
PB/LC
Sp5C
TG
FC Gfap
FC Aif1
FC Cd68
FC Trem2
Sham
Pre-Bregma
Bregma

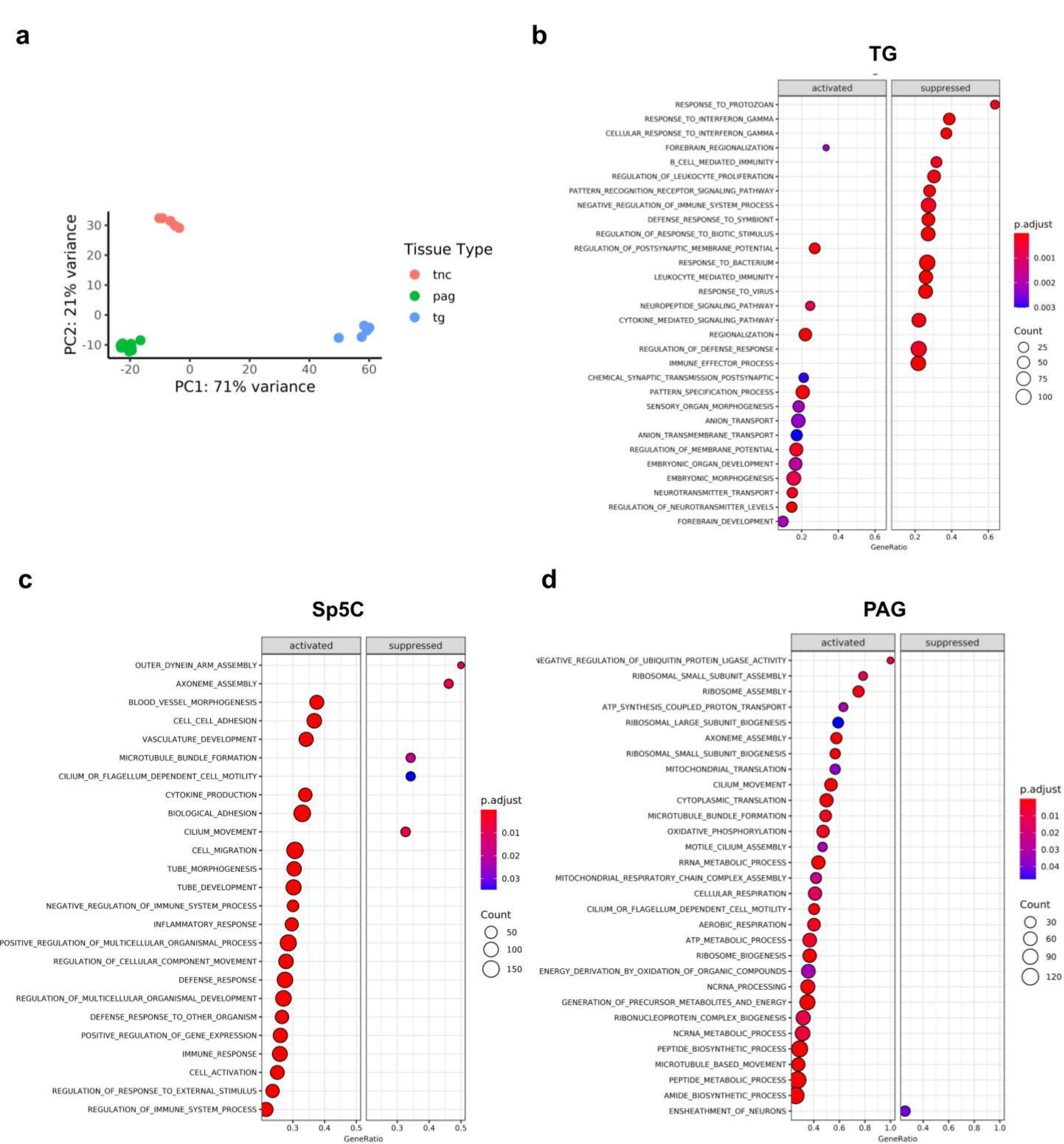
a
PC2: 21% variance
PC1: 71% variance
Tissue Type
tnc
pag
tg
b
TG
activated
suppressed
RESPONSE_TO_PROTOZOAN
RESPONSE_TO_INTERFERON_GAMMA
CELLULAR_RESPONSE_TO_INTERFERON_GAMMA
FOREBRAIN_REGIONALIZATION
B_CELL_MEDIATED_IMMUNITY
REGULATION_OF_LEUKOCYTE_PROLIFERATION
PATTERN_RECOGNITION_RECEPTOR_SIGNALING_PATHWAY
NEGATIVE_REGULATION_OF_IMMUNE_SYSTEM_PROCESS
DEFENSE_RESPONSE_TO_SYMBIONT
REGULATION_OF_RESPONSE_TO_BIOTIC_STIMULUS
REGULATION_OF_POSTSYNAPTIC_MEMBRANE_POTENTIAL
RESPONSE_TO_BACTERIUM
LEUKOCYTE_MEDIATED_IMMUNITY
RESPONSE_TO_VIRUS
NEUROPEPTIDE_SIGNALING_PATHWAY
CYTOKINE_MEDIATED_SIGNALING_PATHWAY
REGIONALIZATION
REGULATION_OF_DEFENSE_RESPONSE
IMMUNE_EFFECTOR_PROCESS
CHEMICAL_SYNAPTIC_TRANSMISSION_POSTSYNAPTIC
PATTERN_SPECIFICATION_PROCESS
SENSORY_ORGAN_MORPHOGENESIS
ANION_TRANSPORT
ANION_TRANSMEMBRANE_TRANSPORT
REGULATION_OF_MEMBRANE_POTENTIAL
EMBRYONIC_ORGAN_DEVELOPMENT
EMBRYONIC_MORPHOGENESIS
NEUROTRANSMITTER_TRANSPORT
REGULATION_OF_NEUROTRANSMITTER_LEVELS
FOREBRAIN_DEVELOPMENT
GeneRatio
p.adjust
Count
c
Sp5C
activated
suppressed
OUTER_DYNEIN_ARM_ASSEMBLY
AXONEME_ASSEMBLY
BLOOD_VESSEL_MORPHOGENESIS
CELL_CELL_ADHESION
VASCULATURE_DEVELOPMENT
MICROTUBULE_BUNDLE_FORMATION
CILIUM_OR_FLAGELLUM_DEPENDENT_CELL_MOTILITY
CYTOKINE_PRODUCTION
BIOLOGICAL_ADHESION
CILIUM_MOVEMENT
CELL_MIGRATION
TUBE_MORPHOGENESIS
TUBE_DEVELOPMENT
NEGATIVE_REGULATION_OF_IMMUNE_SYSTEM_PROCESS
INFLAMMATORY_RESPONSE
POSITIVE_REGULATION_OF_MULTICELLULAR_ORGANISMAL_PROCESS
REGULATION_OF_CELLULAR_COMPONENT_MOVEMENT
DEFENSE_RESPONSE
REGULATION_OF_MULTICELLULAR_ORGANISMAL_DEVELOPMENT
DEFENSE_RESPONSE_TO_OTHER_ORGANISM
POSITIVE_REGULATION_OF_GENE_EXPRESSION
IMMUNE_RESPONSE
CELL_ACTIVATION
REGULATION_OF_RESPONSE_TO_EXTERNAL_STIMULUS
REGULATION_OF_IMMUNE_SYSTEM_PROCESS
GeneRatio
p.adjust
Count
d
PAG
activated
suppressed
NEGATIVE_REGULATION_OF_UBIQUITIN_PROTEIN_LIGASE_ACTIVITY
RIBOSOMAL_SMALL_SUBUNIT_ASSEMBLY
RIBOSOME_ASSEMBLY
ATP_SYNTHESIS_COUPLED_PROTON_TRANSPORT
RIBOSOMAL_LARGE_SUBUNIT_BIOGENESIS
AXONEME_ASSEMBLY
RIBOSOMAL_SMALL_SUBUNIT_BIOGENESIS
MITOCHONDRIAL_TRANSLATION
CILIUM_MOVEMENT
CYTOPLASMIC_TRANSLATION
MICROTUBULE_BUNDLE_FORMATION
OXIDATIVE_PHOSPHORYLATION
MOTILE_CILIUM_ASSEMBLY
RRNA_METABOLIC_PROCESS
MITOCHONDRIAL_RESPIRATORY_CHAIN_COMPLEX_ASSEMBLY
CELLULAR_RESPIRATION
CILIUM_OR_FLAGELLUM_DEPENDENT_CELL_MOTILITY
AEROBIC_RESPIRATION
ATP_METABOLIC_PROCESS
RIBOSOME_BIOGENESIS
ENERGY_DERIVATION_BY_OXIDATION_OF_ORGANIC_COMPOUNDS
NCRNA_PROCESSING
GENERATION_OF_PRECURSOR_METABOLITES_AND_ENERGY
RIBONUCLEOPROTEIN_COMPLEX_BIOGENESIS
NCRNA_METABOLIC_PROCESS
PEPTIDE_BIOSYNTHETIC_PROCESS
MICROTUBULE_BASED_MOVEMENT
PEPTIDE_METABOLIC_PROCESS
AMIDE_BIOSYNTHETIC_PROCESS
ENSHEATHMENT_OF_NEURONS
GeneRatio
p.adjust
Count

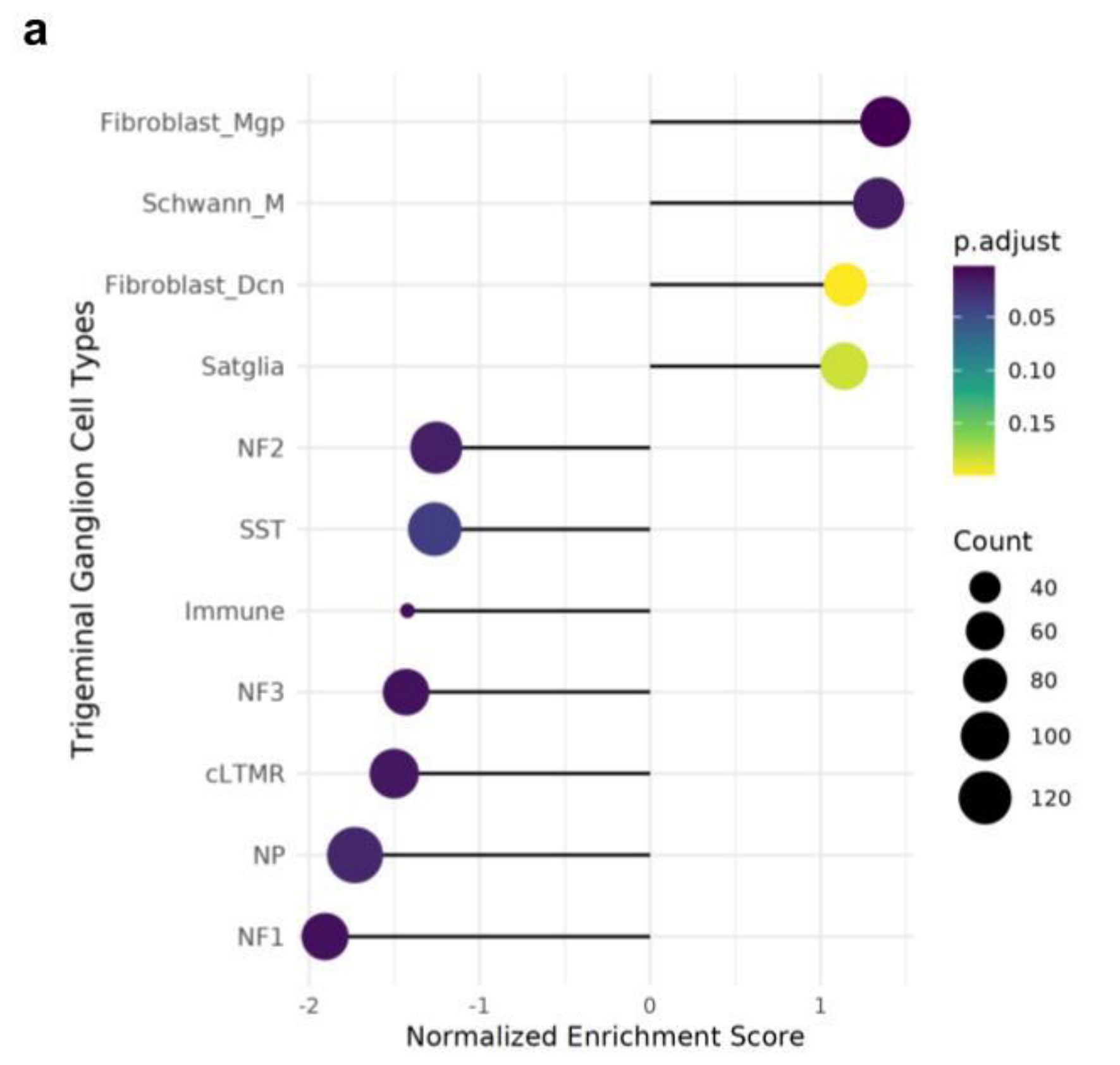
a
Fibroblast_Mgp
Schwann_M
Fibroblast_Dcn
Satglia
NF2
SST
Immune
NF3
cLTMR
NP
NF1
Trigeminal Ganglion Cell Types
-2
-1
0
1
Normalized Enrichment Score
p.adjust
0.05
0.10
0.15
Count
40
60
80
100
120

a

Gfap
Gja1
Slc1a2
**
**
*
*
**
2-ΔΔCt
0
1
2
3
Sham
Day1
Day8
Sham
Day1
Day8
Sham
Day1
Day8
Post TBI Day

b

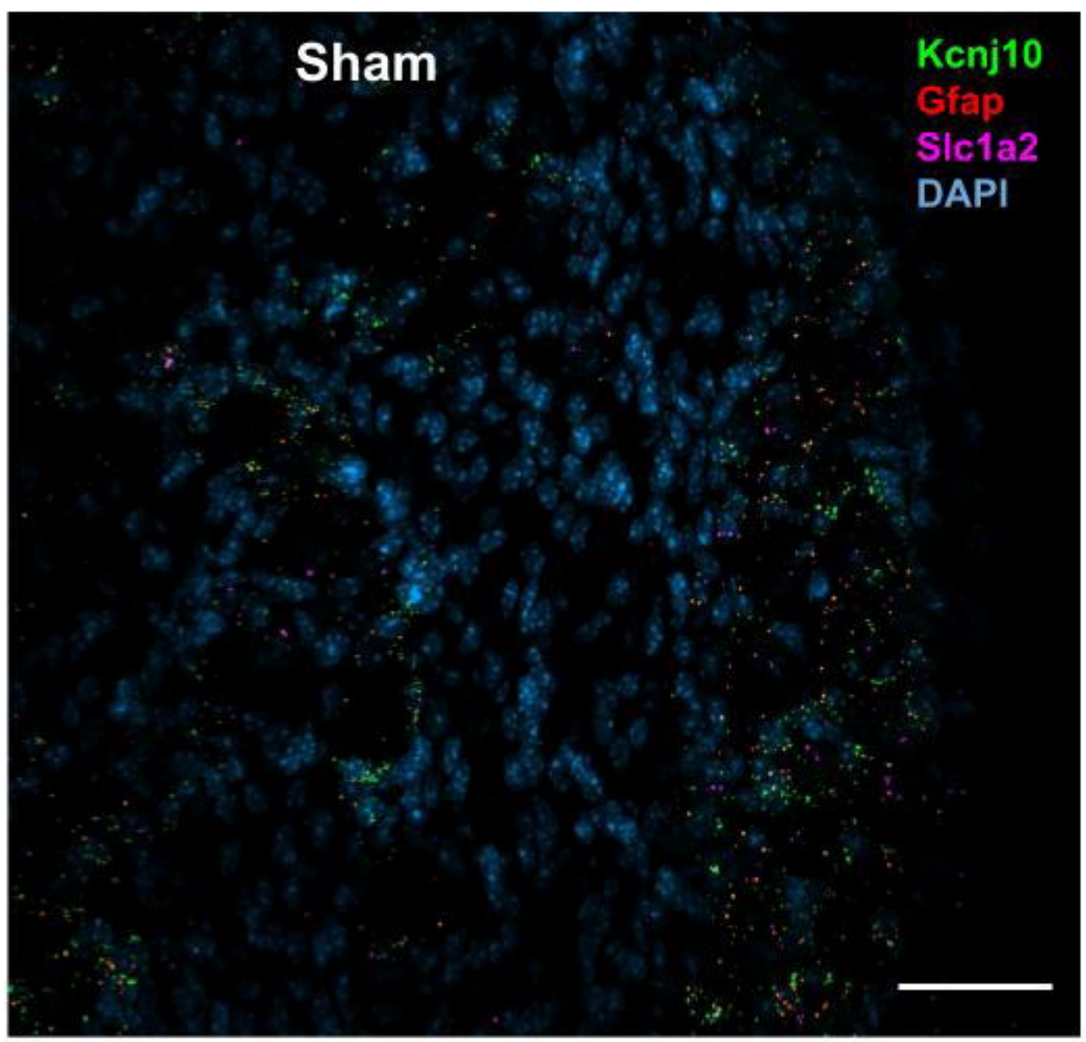
Sham
Kcnj10
Gfap
Slc1a2
DAPI

c

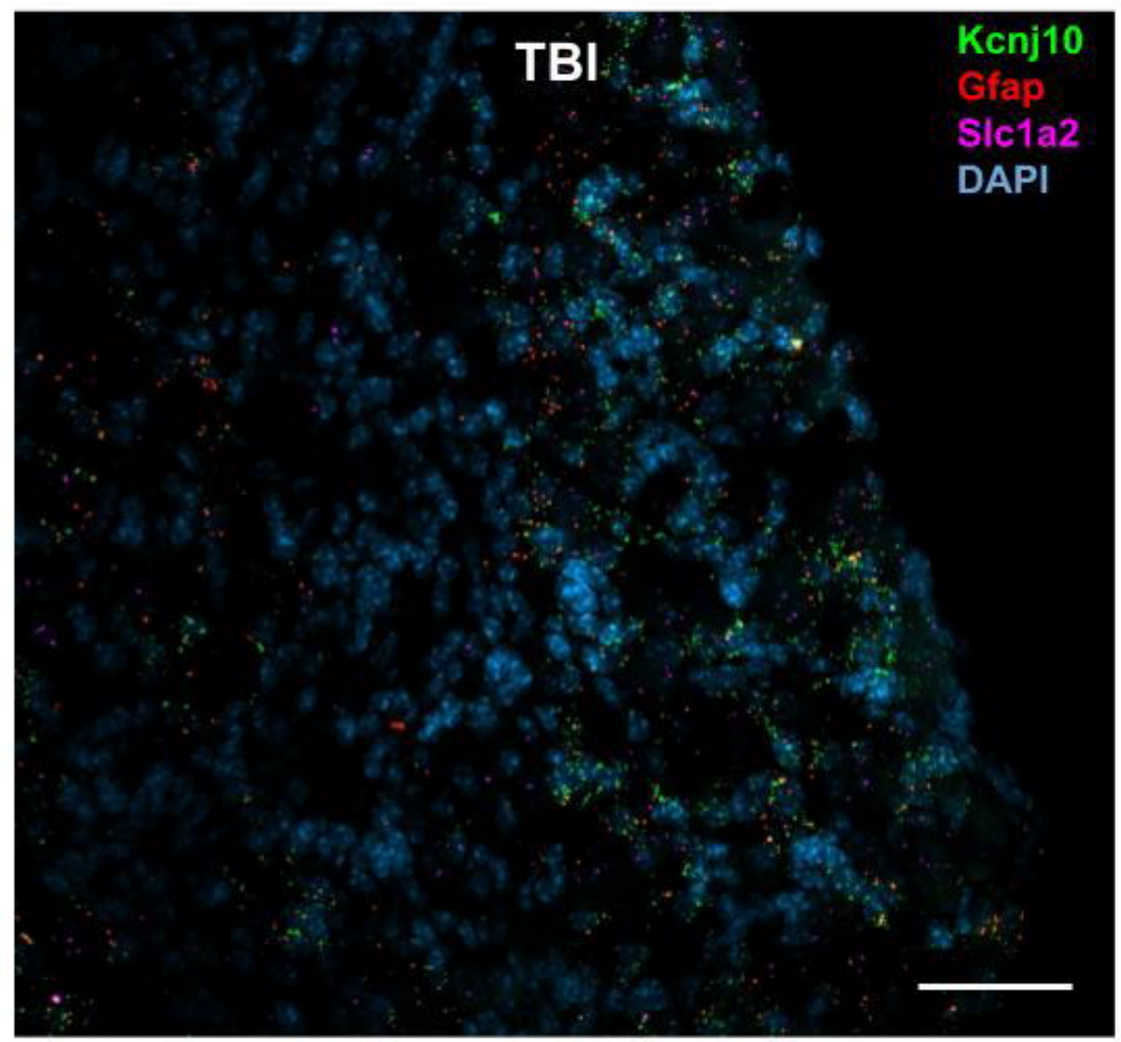
TBI
Kcnj10
Gfap
Slc1a2
DAPI

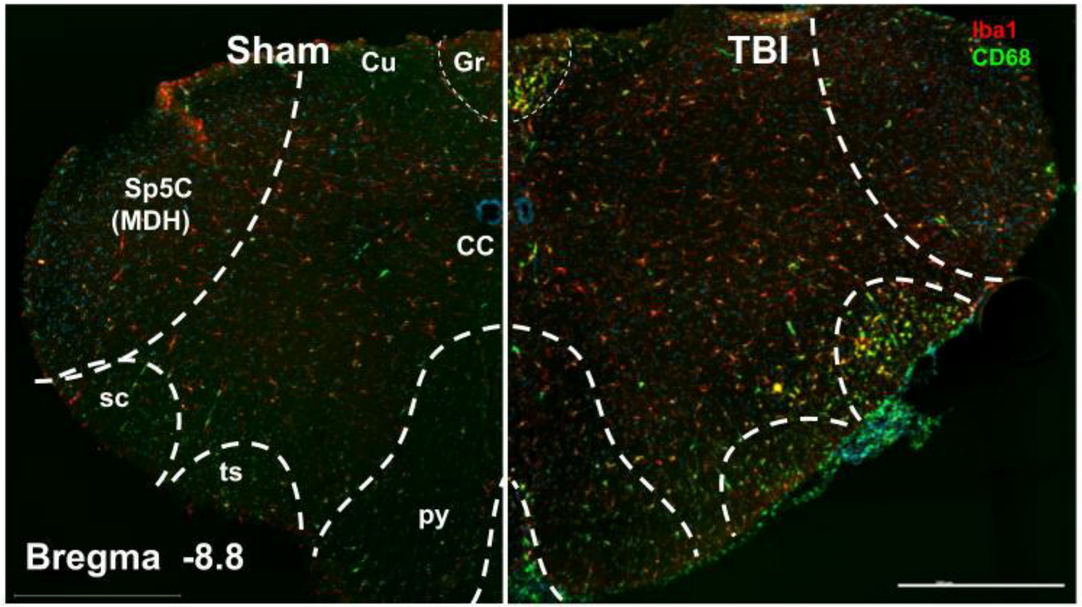
a
Sham
Cu
Gr
Sp5C
(MDH)
CC
sc
ts
py
Bregma -8.8
TBI
Iba1
CD68

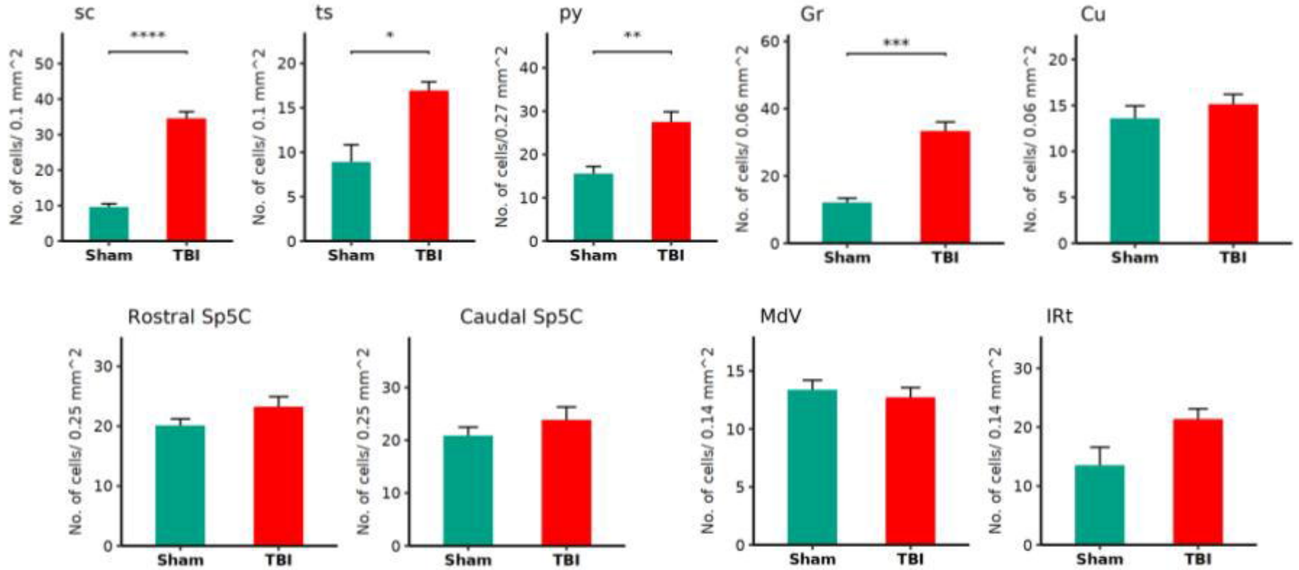
c
sc
ts
py
Gr
Cu
Rostral Sp5C
Caudal Sp5C
MdV
IRt
No. of cells/ 0.1 mm^2
No. of cells/0.27 mm^2
No. of cells/ 0.06 mm^2
No. of cells/ 0.25 mm^2
No. of cells/ 0.14 mm^2
Sham
TBI
****
*
**
***

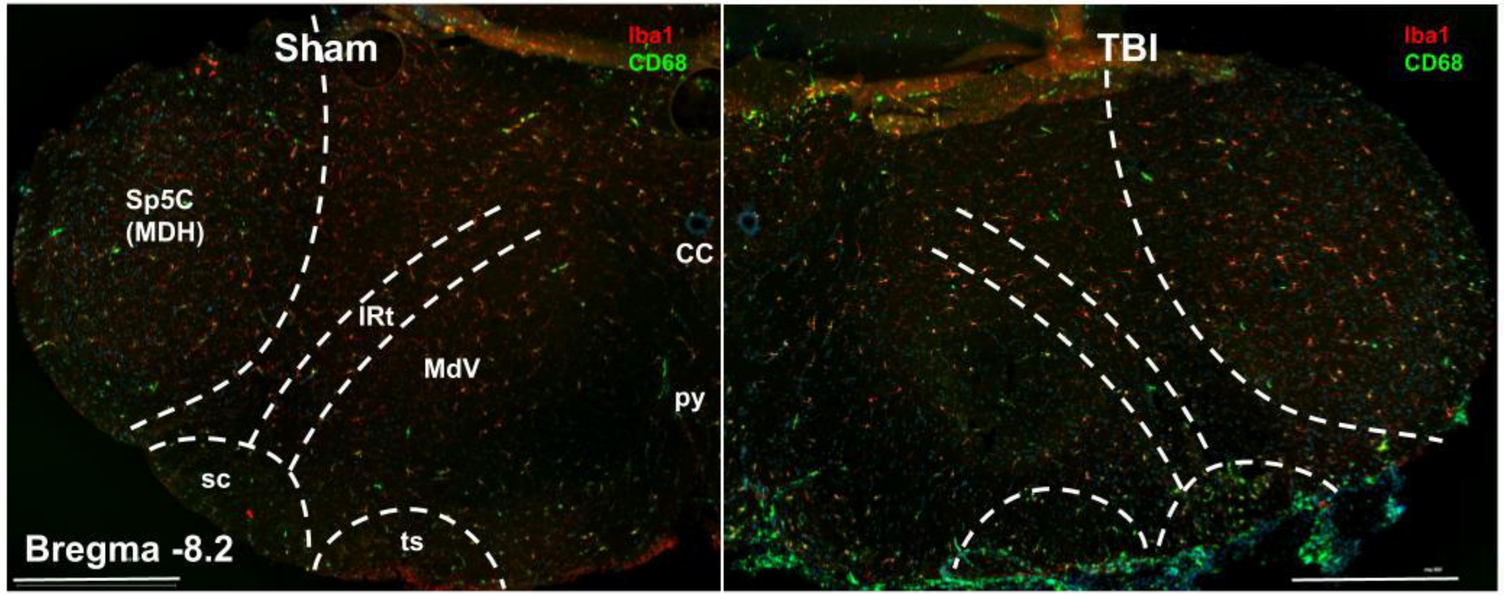
b
Sham
Sp5C
(MDH)
CC
IRt
MdV
py
sc
ts
Bregma -8.2
TBI
Iba1
CD68

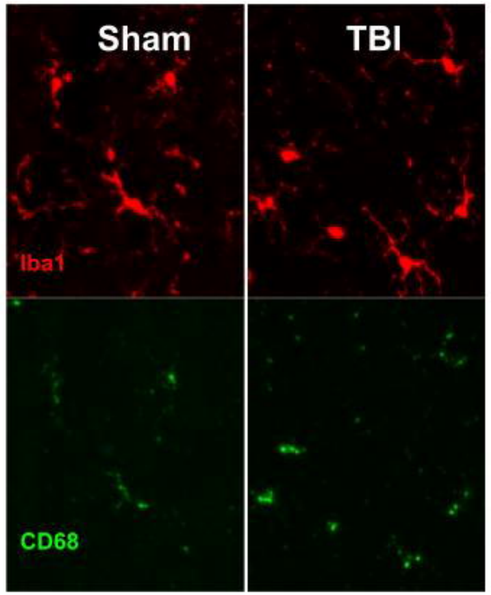
d
Sham
TBI
Iba1
CD68

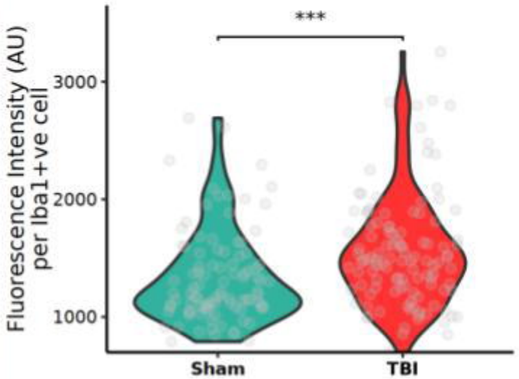
e
Fluorescence Intensity (AU)
per Iba1+ve cell
3000
2000
1000
Sham
TBI
***

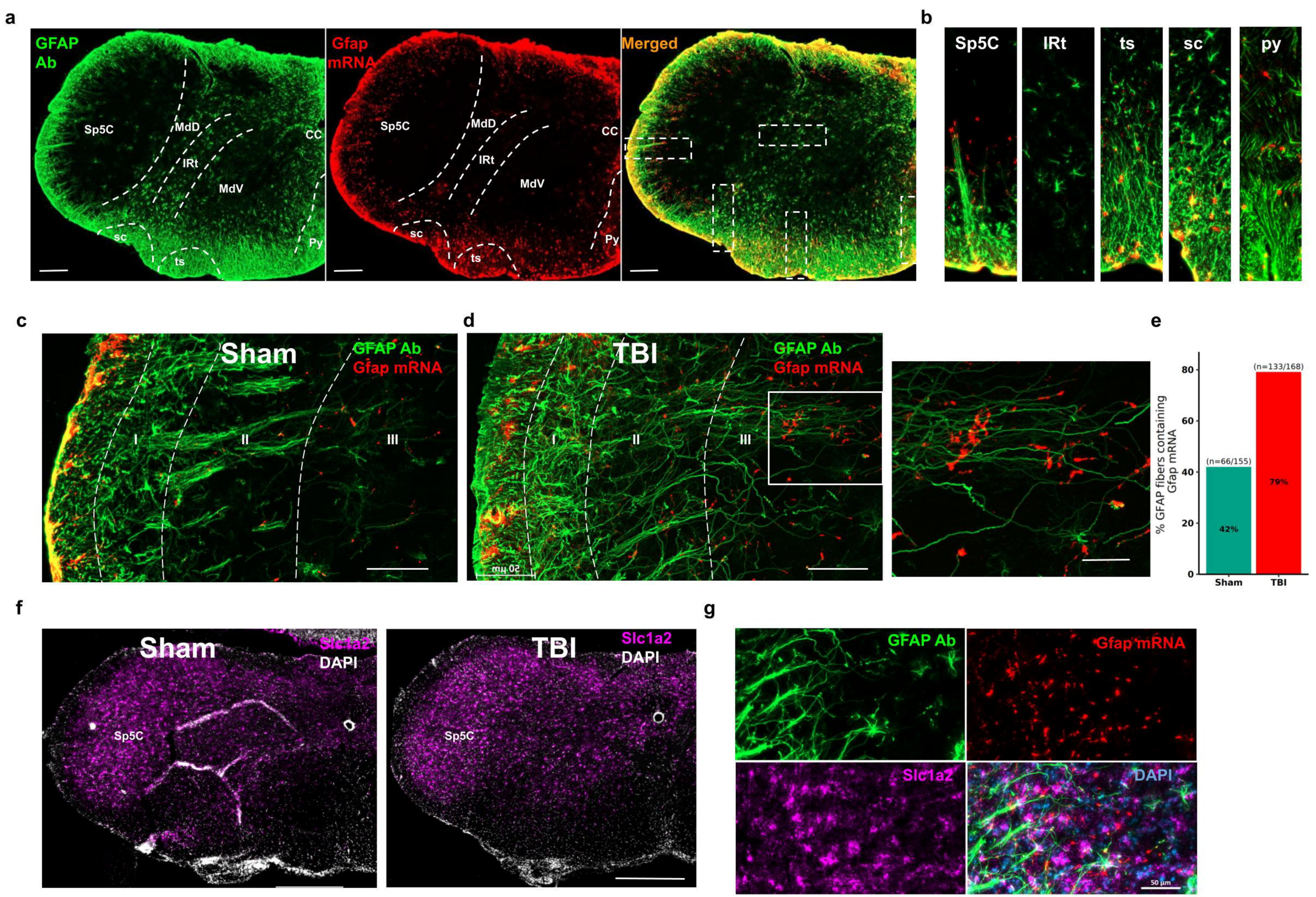
a
GFAP Ab
Gfap mRNA
Merged
Sp5C
MdD
IRt
MdV
CC
sc
ts
Py
b
Sp5C
IRt
ts
sc
py
c
Sham
GFAP Ab
Gfap mRNA
I
II
III
d
TBI
GFAP Ab
Gfap mRNA
I
II
III
20 µm
e
% GFAP fibers containing Gfap mRNA
80
60
40
20
0
(n=133/168)
(n=66/155)
79%
42%
Sham
TBI
f
Sham
Slc1a2
DAPI
Sp5C
TBI
Slc1a2
DAPI
Sp5C
g
GFAP Ab
Gfap mRNA
Slc1a2
DAPI
50 µm

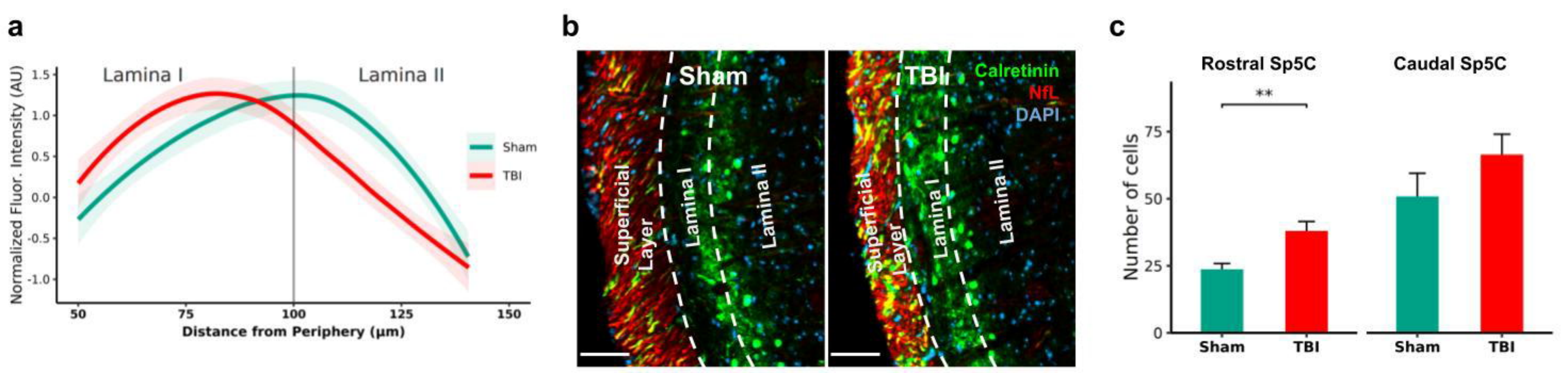
a
Lamina I
Lamina II
Normalized Fluor. Intensity (AU)
1.5
1.0
0.5
0.0
-0.5
-1.0
50
75
100
125
150
Distance from Periphery (µm)
Sham
TBI
b
Sham
TBI
Calretinin
NfL
DAPI
Superficial Layer
Lamina I
Lamina II
c
Rostral Sp5C
Caudal Sp5C
**
Number of cells
75
50
25
0
Sham
TBI
Sham
TBI